Resource

Molecular Cell

An Atlas of Human Glycosylation Pathways Enables Display of the Human Glycome by Gene Engineered Cells

Graphical Abstract

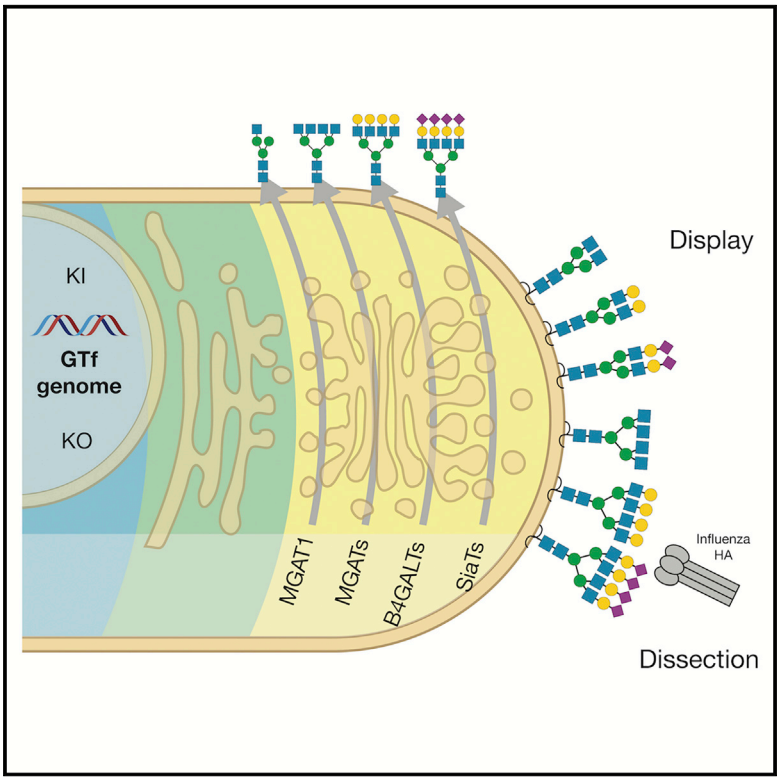

Authors

Yoshiki Narimatsu, Hiren J. Joshi, Rebecca Nason, ..., Sergey Y. Vakhrushev, Zhang Yang, Henrik Clausen

Correspondence

yoshiki@sund.ku.dk (Y.N.), hclau@sund.ku.dk (H.C.)

In Brief

Narimatsu et al. display the diversity of human sugars on the surface of a library of cells by genetically engineering the cellular glycosylation machinery. Sugars on the cell surface play important roles in interactions with the environment, and the cell library developed opens for studies of biological interactions with sugars.

Highlights

- Human glycosyltransferases (170 GTf genes) organized in glycosylation pathway maps
- The human glycome displayed in a natural context on the cell surface
- Sustainable cell-based array resource to dissect biological functions of glycans
- Microbial adhesins may bind to clustered patches of O-glycans

Narimatsu et al., 2019, Molecular Cell *75*, 1–14
July 25, 2019
https://doi.org/10.1016/j.molcel.2019.05.017

CellPress

Please cite this article in press as: Narimatsu et al., An Atlas of Human Glycosylation Pathways Enables Display of the Human Glycome by Gene Engineered Cells, Molecular Cell (2019), https://doi.org/10.1016/j.molcel.2019.05.017

Molecular Cell
Resource

An Atlas of Human Glycosylation Pathways Enables Display of the Human Glycome by Gene Engineered Cells

Yoshiki Narimatsu,[1,2,*] Hiren J. Joshi,[1] Rebecca Nason,[1] Julie Van Coillie,[1] Richard Karlsson,[1] Lingbo Sun,[1] Zilu Ye,[1] Yen-Hsi Chen,[1,2] Katrine T. Schjoldager,[1] Catharina Steentoft,[1] Sanae Furukawa,[1] Barbara A. Bensing,[3] Paul M. Sullam,[3] Andrew J. Thompson,[4] James C. Paulson,[4,5] Christian Büll,[1,6] Gosse J. Adema,[6] Ulla Mandel,[1] Lars Hansen,[1] Eric Paul Bennett,[1] Ajit Varki,[7] Sergey Y. Vakhrushev,[1] Zhang Yang,[1,2] and Henrik Clausen[1,8,*]

[1]Copenhagen Center for Glycomics, Departments of Cellular and Molecular Medicine and Odontology, Faculty of Health Sciences, University of Copenhagen, Blegdamsvej 3, Copenhagen, Denmark

[2]GlycoDisplay ApS, Copenhagen, Denmark

[3]Department of Medicine, The San Francisco Veterans Affairs Medical Center, and the University of California, San Francisco, San Francisco, CA 94121, USA

[4]Department of Molecular Medicine, The Scripps Research Institute, La Jolla, CA, USA

[5]Department of Immunology and Microbiology, The Scripps Research Institute, La Jolla, CA, USA

[6]Radiotherapy and OncoImmunology Laboratory, Department of Radiotherapy, Radboud University Medical Center, Nijmegen, the Netherlands

[7]The Glycobiology Research and Training Center and the Department of Cellular and Molecular Medicine, University of California, San Diego, San Diego, CA 92093, USA

[8]Lead Contact

*Correspondence: yoshiki@sund.ku.dk (Y.N.), hclau@sund.ku.dk (H.C.)

https://doi.org/10.1016/j.molcel.2019.05.017

SUMMARY

The structural diversity of glycans on cells—the glycome—is vast and complex to decipher. Glycan arrays display oligosaccharides and are used to report glycan hapten binding epitopes. Glycan arrays are limited resources and present saccharides without the context of other glycans and glycoconjugates. We used maps of glycosylation pathways to generate a library of isogenic HEK293 cells with combinatorially engineered glycosylation capacities designed to display and dissect the genetic, biosynthetic, and structural basis for glycan binding in a natural context. The cell-based glycan array is self-renewable and reports glycosyltransferase genes required (or blocking) for interactions through logical sequential biosynthetic steps, which is predictive of structural glycan features involved and provides instructions for synthesis, recombinant production, and genetic dissection strategies. Broad utility of the cell-based glycan array is demonstrated, and we uncover higher order binding of microbial adhesins to clustered patches of O-glycans organized by their presentation on proteins.

INTRODUCTION

The great structural diversity and complexity of the glycome of cells pose huge challenges for analytic and functional studies to extract and define specific biological roles and the underlying molecular basis. Glycan arrays have played a pivotal role in surveying and mapping the informational content of complex glycans. Different strategies have been undertaken to immobilize and display libraries of glycans in printed array formats, drawing parallels to DNA arrays (Rillahan and Paulson, 2011), and approaches to produce comprehensive oligosaccharide libraries vary from chemical and chemoenzymatic synthesis to isolation of natural oligosaccharides and glycoconjugates. Different immobilization strategies have been used, with the most prevalent being coupling to *N*-hydroxysuccinimide (NHS)-activated slides and the neoglycolipid approach utilizing reductive amination to link released oligosaccharides to an amino-phospholipid (Blixt et al., 2004; Fukui et al., 2002; Palma et al., 2014; Puvirajesinghe and Turnbull, 2016). Two larger academic initiatives host these resources and offer services for the scientific community (www.functionalglycomics.org and www.imperial.ac.uk/glycosciences/). These glycan arrays are utilized with great success to probe glycan binding specificities of lectins and microbial adhesins; in particular, the Consortium for Functional Glycomics arrays and expanded sialoside microarrays have been instrumental in dissecting the subtle binding specificities of different influenza hemagglutinins (HAs) and their role in cross-species transmission (Padler-Karavani et al., 2012; Peng et al., 2017; Rillahan and Paulson, 2011; Wang et al., 2013). Glycan array technology depends on continued synthesis and/or isolation of glycans and often requires larger community-supported efforts. There are limitations in the size and complexity of glycans that can be synthesized and in impact of the linkers used (Padler-Karavani et al., 2012; Rillahan and Paulson, 2011). Perhaps the most important limitation is the unnatural context in which the oligosaccharides or neoglycolipids are

displayed in high densities without context of the protein or lipid backbone to which the glycans are normally attached (Blixt et al., 2004), as well as interactions with adjacent glycans that have been suggested to generate ''clustered saccharide patches'' (Cohen and Varki, 2014; Varki, 1994). Printed glycan arrays do not display glycans as they are found on the cell surface, and they most often report a complex collection of glycan hapten structures with limited guidance for further studies.

While the human glycome is vast, the cellular glycosylation machinery producing this diversity is simpler and, arguably, better understood and approachable. The human genome contains over 200 distinct genes encoding glycosyltransferases, and the knowledge of their properties of these and their roles in the 15 known distinct glycosylation pathways in human cells is relatively advanced (Joshi et al., 2018a). Clearly, orchestration of the human glycome involves a large number of additional enzymes, including those that modify glycans such as sulfotransferases and epimerases, transporters, and other proteins; and the glycosylation processes involve overlapping, competing, and intertwined reactions, in particular, by families of isoenzymes that may be difficult to predict. However, to a large extent, the general scaffolds and structures of the glycome may be predicted from the repertoire of only 153 glycosyltransferase genes, as proposed in Figures 1, S1, and S2. The glycosylation pathway maps organize glycosyltransferase genes into pathway-specific and pathway-nonspecific steps in the biosynthesis of distinct glycoconjugates, and illustrates potential redundancies for individual biosynthetic steps provided by isoenzymes and alternative competing biosynthetic steps. These maps provide predictions of structural glycan features affected by the presence or absence of individual genes and whether global or differential subtle outcomes are expected. Combined with the recent introduction of the facile nuclease-based gene-editing tools (Steentoft et al., 2014), we posit that it is now timely and conceivable to take an entirely genetic approach to dissect and display the structural diversity of the glycome of a human cell. Clearly, the glycosylation pathway maps require continuous refinement with increased insight into nonredundant and competing functions of isoenzymes, which requires further studies in isogenic cell models with combinatorial engineering to evaluate outcome. This has been a fruitful strategy for the discovery of functions of the large family polypeptide GalNAc-transferase isoenzymes controlling O-glycosylation (Schjoldager et al., 2015). To begin to facilitate such comprehensive gene targeting, we previously generated a validated CRISPR/Cas9 guide RNA (gRNA) library for highly efficient knockout (KO) targeting of all human glycosyltransferase genes (Narimatsu et al., 2018) and strategies for stable, site-specific knockin (KI) of non-expressed genes (Yang et al., 2015b).

Genetic approaches studying the biology of glycans have a long history. A large collection of Chinese hamster ovary (CHO) cell lines was originally developed through chemical mutagenesis and selection for loss of lectin binding or expression of cell-surface proteins (Conzelmann and Kornfeld, 1984; Kingsley et al., 1986; Patnaik and Stanley, 2006), and most of these cells have been characterized to have defects in a distinct glycosyltransferase gene, donor sugar nucleotide synthase gene, sugar nucleotide transporter, or sugar nucleotide epimerase gene, with resulting loss or gain of global glycan features such as complex N-glycans, complete loss of sialylation or fucosylation of all glycans, or complete loss of glycosaminoglycan structures. These mutant cells have been important tools for determining the requirement for global glycan features, but they do not enable deeper insight into glycan structures involved in biological interactions. Studies of deficiencies in glycosylation genes with rodents have also illustrated the wide biological importance of glycans and the glycosylation process (Lowe and Marth, 2003), while in humans, a large number of congenital disorders of glycosylation (CDGs) have contributed substantially to our understanding of the importance of many different types of glycosylation (Ng and Freeze, 2018). In many cases, the complexities of whole-organism-level analyses have precluded identification of specific structure-function relationships. Past studies with mutant cell lines and organisms clearly demonstrate the power of genetic approaches to probe the glycome, and perhaps one of the best illustrations hereof is the complete unraveling of the many genes necessary for biosynthesis of the extraordinarily complex O-mannose glycan structure required for laminin binding to α-dystroglycan (Jae et al., 2013). This and more recent studies using precise gene engineering to delineate and reprogram glycosylation pathways in mammalian cell lines demonstrate the ability to dissect biological roles of glycosylation genes and their contribution to the glycome (Lavrsen et al., 2018; Schulz et al., 2018; Stolfa et al., 2016; Yang et al., 2015b). These studies also show that genetic reprogramming of glycosylation can be performed with a high degree of predictability.

Here, we apply a fairly comprehensive genetic ''tree-pruning'' approach—glycotopiary—to engineer and reprogram the glycosylation capacities of a human cell line in order to construct a cell-based glycan array that covers a large part of the structural diversity of the human glycome. We used a rational combinatorial approach to eliminate and/or introduce *de novo* glycosylation capacities to develop sublibraries of stably engineered HEK293 isogenic cells that individually display the loss or gain of distinct features of the human glycome. Importantly, combinatorial engineering of isoenzyme families with poorly understood functions enabled dissection and display of uniquely regulated glycan features. We demonstrate performance of the array with a series of plant, microbial, and human lectins. We confirmed the hypothesis that the glycoconjugate and cellular context of glycans provide additional and necessary diversity in structural permutations of the human glycome. Cell-based array analysis of avian and human influenza virus HAs fully recapitulated the known selective binding to α2-3 or α2-6-linked sialic acids (SAs) (Rillahan and Paulson, 2011), and the added context of the cell provided evidence for binding selectivities beyond the simple SA linkage. Analysis of streptococcal serine-rich repeat adhesins produced refinement of the recognized O-glycan structures, compared to information derived from printed glycan arrays, providing evidence for the recognition of clusters or patterns of O-glycans created by the protein carrier. Thus, the cell-based glycan array fully complements the traditional printed glycan arrays and further provides insight into the genetic and biosynthetic regulation of glycan recognition events, with broader context of glycoconjugate nature and higher order presentation.

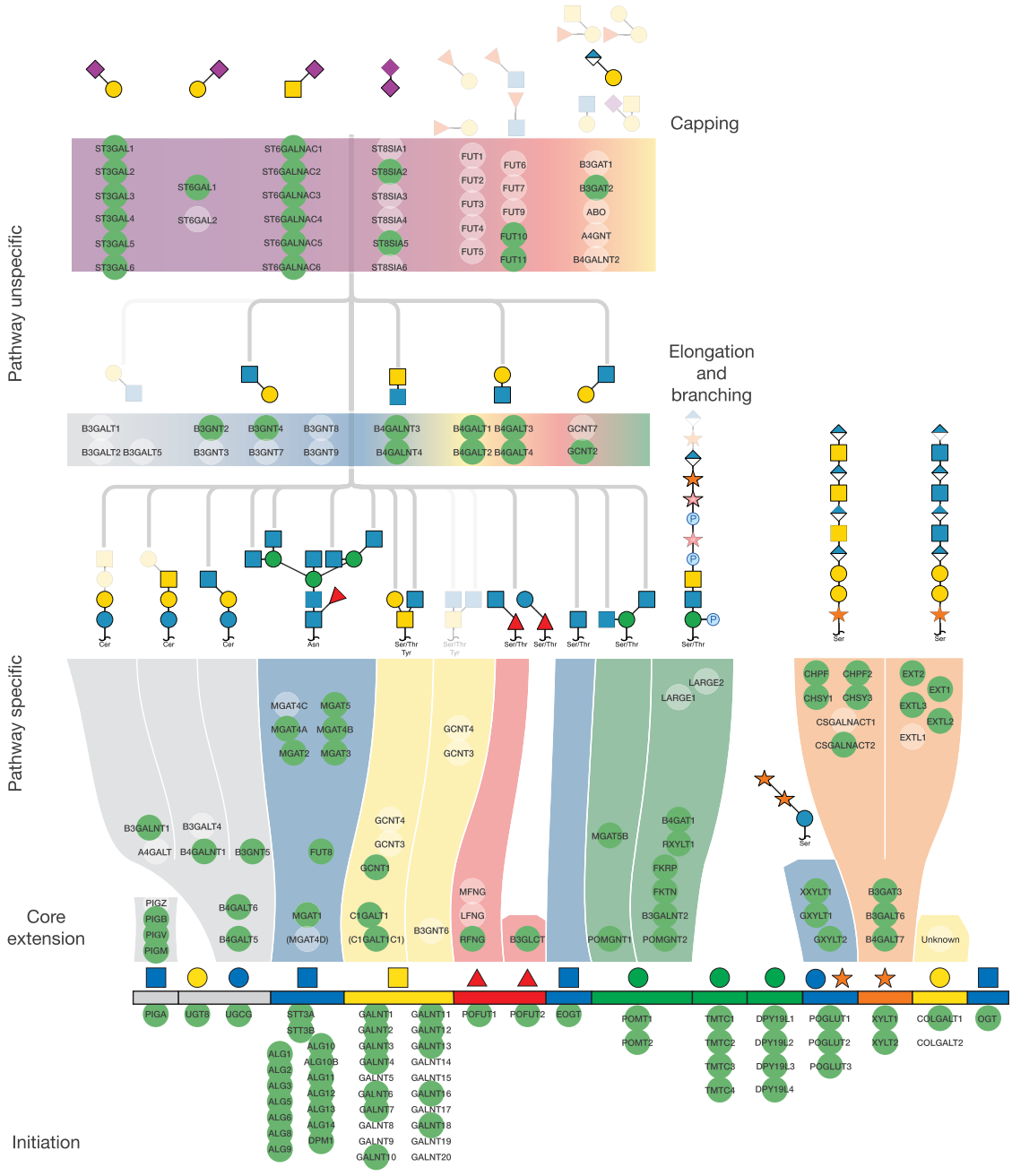

Figure 1. An Atlas of Human Glycosylation Pathway Maps with Assigned Functions of 169 Glycosyltransferase Genes

Rainbow depiction of the 15 distinct human glycosylation pathways including, from left to right: GPI-anchor, glycolipids (two pathways), N-linked glycans, O-GalNAc mucin-type, O-Fuc type (two pathways), O-GlcNAc type (epidermal growth factor; EGF), O-Man type (POMT-directed), O-Man type (TMTC-directed), C-Man type, O-Glc type, O-Xyl type (proteoglycans), O-Gal type (collagen), and O-GlcNAc type (cytosolic). The basic structural features of oligosaccharides for most glycosylation pathways are shown above each rainbow segment, and the common glycan structures found on these 15 different types of glycosylation with the predicted functions of individual GTf-genes in biosynthetic steps are illustrated in Figure S2. Glycosyltransferase genes are arranged in the pathway-specific initiation and core extention steps (117 genes) and in pathway-nonspecific elongation and capping steps (52 genes). Genes circled by green are predicted to be expressed in HEK293 cells based on RNA-seq analysis, and the predicted basic glycan features missing in HEK293 cells are faded out. Glycan symbols are drawn according to the SNFG format (Varki et al., 2015a).

RESULTS

The Glycotopiary Strategy

We organized current knowledge of 169 glycosyltransferase genes directing the human glycome into a rainbow diagram that organizes these genes into the 15 distinct glycosylation pathways symbolized by the color used for the first monosaccharide (Figure 1; Joshi et al., 2018a, 2018b; Narimatsu et al., 2018), with the predicted functions in biosynthetic steps and pathways as shown in Figure S2. 44 genes can be assigned to pathway-specific functions in the initiation of glycosylation of different types of glycoconjugates, 16 genes can be assigned to assembly of the lipid-linked oligosaccharide precursor and oligosaccharyltransferase dedicated to N-glycosylation, and 57 genes can be assigned to pathway-specific functions in immediate core extension and branching steps. Thus, 117 of the 169 genes are assignable to distinct glycosylation pathways, and several of these predictions were previously validated with CHO mutant cells (Patnaik and Stanley, 2006), targeted CHO KO cells (Yang et al., 2015b), and other mammalian cell lines (Stolfa et al., 2016). We classified 17 genes to pathway-nonspecific elongation or branching and another 35 genes to pathway-nonspecific capping, including sialylation and fucosylation. While it is possible to reliably assign most of the glycosyltransferases that belong to the large isoenzyme families to general biosynthetic steps, it is important to note that, for most of these isoenzymes, our understanding of their specific non-redundant functions is still very limited. We previously demonstrated how genetic KO and/or KI dissection of isoenzyme genes can be used to identify non-redundant functions of isoenzymes (Schjoldager et al., 2015), and this is clearly the strategy needed to dissect the large β3/4Gal-transferase, β3GlcNAc-transferase, and α2-3 or α2-6 sialyltransferase isoenzyme families. We previously also classified human glycosyltransferase genes grossly into regulated and non-regulated based on organ transcriptome data (Joshi et al., 2018a), and this provides indications of differentially regulated glycosylation steps and pathways that contribute to the diversity of the glycome.

We selected the HEK293 cell line as the platform for construction of the cell-based glycan display because structural analyses of different types of glycans suggest a high degree of complexity in glycosylation (Fujitani et al., 2013; Termini et al., 2017; Yang et al., 2012), and this cell line is widely used for recombinant expression and characterization of glycoproteins (Thomas and Smart, 2005). We used RNA-sequencing (RNA-seq) transcriptomics as a rough prediction of the glycosylation capacity of HEK293 cells, and 121 of the 169 glycosyltransferase genes had detectable transcripts (fragments per kilobase million [FPKM] $\geq$ 1), while 47 were not or were poorly detectable (FPKM < 1) (Figure S1). Figure 1 illustrates the glycosyltransferase genes predicted to be expressed and their proposed functions, and the interpretation largely correlates with reported structural analysis (Yang et al., 2012). Thus, HEK293 cells are predicted to have the capacity for all types of lipid and protein glycosylation, comprehensive elaboration of pathway-specific elongation and branching features, type 2 chain LacNAc and GalNAcβ1-4GlcNAc (LacDiNAc) core chains, and both α2-3 and α2-6SA capping. SA in HEK293 is primarily Neu5Ac, unless cells are cultured in bovine serum from where Neu5Gc can be scavenged, and acetylation has been reported (Wasik et al., 2017). The limited glycan features not predicted to be produced in HEK293 cells are globoseries glycosphingolipids (*A4GALT*); core1 extended (*B3GNT3*) and core3/4 branched GalNAc-type O-glycans (*B3GNT6*, *GCNT3*, and *GCNT4*); type 1 chain N-acetyl-lactosamine (LacNAc) structures (*B3GALT1*, *T2*, *T4*, and *T5*); and capping by blood group ABH, Sda, and Lewis antigens (*ABO*, *B4GALNT2*, *FUT1*, *FUT2*, and *FUT3*). Moreover, the capacity for α3 fucosylation and α2-8 sialylation is predicted to be low or absent, due to the limited expression of members of the large isoenzyme FUT and ST8SIA families.

The basic glycotopiary concept to add and remove branches of glycan complexity by genetic KO and/or KI of glycosyltransferase genes, in order to generate isogenic cells displaying loss or gain of particular glycosylation features, is presented in Figure 2A. This illustrates how combinatorial CRISPR/Cas9 KO targeting of the genes controlling the earliest essential steps in elongation or elaboration of glycans found on glycosphingolipids (*B4GALT5/6*), N-glycoproteins (*MGAT1*), and GalNAc-type O-glycoproteins (*C1GALT1/COSMC*) results in isogenic cells differentially displaying glycan features on one or more of these glycoconjugates. The performed KO and/or KI targeting is indicated by red and green dots, respectively, with lines between dots representing combinatorial gene engineering.

A Sublibrary Strategy to the Cell-Based Glycan Array

We designed sublibraries with the capacity to differentially display defined glycan features grouped according to the rainbow biosynthetic scheme (Figure 2B). The sublibraries consist of groups of isogenic cells with reprogrammed glycosylation capacities for the major steps in glycosylation. Sublibrary 1 was designed to differentially display the major types of glycoconjugates by eliminating the earliest pathway-specific elongation steps for one or more glycoconjugates, resulting in the display of N-glycans (KO *MGAT1*), GalNAc-type O-glycans (KO *COSMC*), and/or glycosphingolipids (KO *B4GALT5/6*), as well as independently Man-type O-glycans (KO *POMGNT1*, *POMGNT2*, and *TMTC1-4*) and glycosaminoglycans (GAGs) (KO *B4GALT7*). Sublibraries 2–5 differentially display most pathway-specific glycan features separately for glycosphingolipids, N-glycan branching, GalNAc-type O-glycan branching, and GAG core structures, respectively. Sublibrary 6 differentially displays pathway-nonspecific elongation by type 2 chain LacNAc and/or LacDiNAc and poly-LacNAc. Sublibraries 7 and 8 differentially display pathway-nonspecific Gal capping by α2-3 and/or α2-6SA, as well as GalNAc capping by α2-6SA. Importantly, the individual and combinatorial targeting of isoenzyme genes enables the display of the contribution of individual isoenzymes to the glycome and the dissection of their unique non-redundant functions and interpretation of the underlying structural glycan features (Schjoldager et al., 2015).

We used site-directed KI integration of human glycosyltransferase genes to introduce glycan features not endogenously expressed in HEK293 cells. These cells do not express the complex GalNAc-type core3/4 O-glycans, which are generally poorly expressed in cancer cell lines. The core3 pathway competes

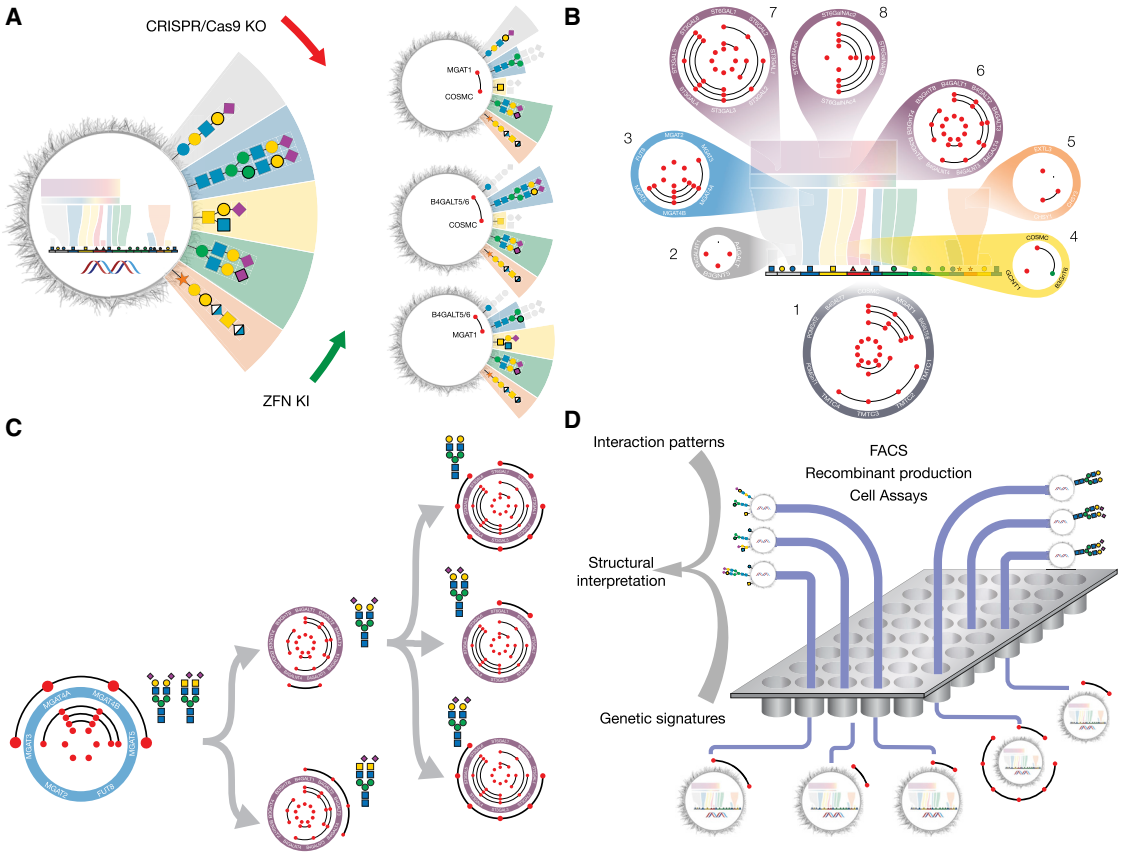

Figure 2. Design and Construction of a Cell-Based Display Platform for the Human Glycome

(A) Depiction of the KO and/or KI gene engineering strategy for the development of isogenic HEK293 cells with selective loss or gain of glycosylation capacities. Illustrated is how early combinatorial KO (red dots connected by a black line) of the glycosyltransferase genes controlling the early steps in glycosphingolipid glycosylation (*B4GALT5/6*), N-glycosylation (*MGAT1*), or GalNAc-type O-glycosylation (*C1GALT1/COSMC*) generate cells with and without elaborated glycan features found on these glycoconjugates. The depicted glycan structures and outcomes of the engineering are simplified to illustrate the truncation effects by graying out.

(B) Depiction of a sublibrary cell strategy for display of glycan features with sublibraries (1–8) covering the principal pathway-specific and pathway-nonspecific glycosylation steps that enable differential display of the following key features: (1) type of glycoconjugates; (2) type of glycosphingolipids; (3) branching and core fucose of N-glycans; (4) core of GalNAc-type O-glycans; (5) chondroitin/dermatin (CS/DS) and heparan sulfate (HS) GAGs; (6) core structures LacNAc and LacDiNAc; (7) capping by α2-3 and α2-6SA; and (8) sialylation by α2-6SA. Red dots in circles of sublibraries represent KO of a glycosyltransferase gene, with combinatorial KO indicated by lines between genes. Green dots represent KI of a glycosyltransferase gene not endogenously expressed in HEK293 cells.

(C) Design of sublibrary connectivities for the display of distinct complex glycan features. Illustrated is the design strategy used to differentially display homogeneous N-glycans with LacNAc or LacDiNAc elongation and α2-3 or α2-6SA capping. A biantennary N-glycan design (sublibrary 3) was combined with LacNAc or LacDiNAc designs (sublibrary 6) and α2-3SA, α2-6SA, or no SA designs (sublibrary 7). A complete summary of the current status of sublibraries and connectivities generated is presented in Table S1.

(D) Graphic depiction of experimental workflows using the cell-based array. Libraries of isogenic cells with known genetic engineering and display of distinct subsets of the human glycome may be used in diverse bioassays and for recombinant production of reporter glycoconjugates for further studies and validation. The readouts of these assays generate patterns of interactions (loss or gain), e.g., binding intensities quantified by flow cytometry, and these patterns are translated using the atlas of glycosylation maps (Figure 1) into structural glycan motifs and types of glycoconjugates. Interaction patterns typically include multiple informative data points due to the sequential nature of oligosaccharide biosynthesis to strengthen the structural interpretations. Sequential use of sublibraries and additional connectivity engineering are used to simplify workflow and for refinement.

See also Figures S3, S5, and S6.

with core1, so we generated a stable KI of the core3 synthase (*B3GNT6*) in HEK293 cells with a KO of the core1 (*COSMC*). The important cancer-associated STn O-glycan is not endogenously displayed in HEK293 cells, even after KO of *COSMC* (Steentoft et al., 2011), so we used a KI of *ST6GALNAC1* in cells with KO of *COSMC* to induce homogeneous display of STn. We also used a KI of dominating glycosyltransferases (*ST3GAL4*, *ST6GAL1*, and *GCNT1*) to enhance the corresponding glycan features.

Connectivity of Sublibraries for Fine Dissection

The sublibraries display glycan features independently of each other, and further engineering is required to connect results obtained by individual libraries. As an example, Figure 2C illustrates

how a specific design from the N-glycan branching sublibrary 3 (biantennary N-glycan) is connected with designs from the LacNAc or LacDiNAc sublibrary 6 (biantennary N-glycan with LacNAc or LacDiNAc), and, ultimately, with the α2-3/2-6SA sublibrary 7, to display biantennary LacNAc N-glycans capped with and without α2-3 or α2-6SA. This strategy for connecting sublibraries enables the display of biantennary N-glycans without LacDiNAc capped with only α2-3SA, as validated by N-glycan profiling of total cell lysates and with a N-glycoprotein reporter construct (Figure S3B). Such combinatorial connectivity between sublibraries will be needed to cover and dissect the complete glycoconjugate context, and this should be carried out during the pursuit of interesting specific biological interactions where multiple positive or negative data points are used to build and validate the entire glycoconjugate structure required for biological interactions, as illustrated later. The current state of the cell library, including combinatorial engineering across sublibraries, is addressed in Table S1.

Figure 2D illustrates the principles, workflow, and some applications of the cell-based glycan array. Individual cells from sublibraries of isogenic HEK293 cells with reprogrammed glycosylation are used in different biological assays amenable with live or fixed cells. Here, we used flow cytometry to interrogate the glycosyltransferase gene(s) that affect the outcome of the assay used. The cell-based array will report patterns of reactivities (positive, negative, or none) with libraries of engineered isogenic cells, and these data points, together with the atlas of glycosylation pathways, are used to interpret the structural features of glycans and potential specific glycoconjugates involved (Figure 1). In striking contrast to the traditional printed glycan arrays, the cell-based array provides information regarding the genetic and biosynthetic regulation of the target glycan, as well as instructions for production of the relevant target and a ready engineered host cell for this. The approach will generally bring multiple independent data points that support the structural interpretation of the involved glycan, because glycosylation is a step-by-step process. It is important to recognize the power of reinforcement provided by the complementarity and plurality of data points from sequential steps in the glycosylation pathways, as well as the discovery power of seemingly common glycan hapten structures that may be differentially regulated by individual isoenzymes on specific scaffold structures or types of glycoconjugates.

Validating the Cell-Based Glycan Array

The glycosylation capacities of HEK293^{WT} cells have been probed previously by N- and O-glycan profiling of total cell lysates and recombinant expressed glycoproteins (Fujitani et al., 2013; Termini et al., 2017; Yang et al., 2012), demonstrating expression of glycan features in excellent agreement with the predictions made from transcriptome analysis (Figure S1). These included high-mannose (high-Man) and multiantennary complex type N-glycans with and without LacNAc and/or LacDiNAc and/or core Fuc and with both α2-3 and α2-6SA, while O-glycans included core1 and core2 structures with SA. Here, we confirmed and extended this by N-glycan and GAG profiling of total cell lysates from HEK293^{WT}, as well as site-specific analysis of recombinant expressed N- and O-GalNAc glycoprotein reporters (Figure S3; Table S2). It is a daunting, largely unnecessary, and, to some extent, impossible task to undertake detailed structural analysis of the outcomes of all the extensive glycoengineering performed. In particular, it is currently essentially impossible to capture the fine structural features involved in particular biological interactions at the cell membrane through analysis of the glycome of whole cells. The cell-based array is, in contrast, ideal for this task. The array is designed to report the genetic and biosynthetic basis for interactions with glycan features on the cell surface, and the positive or negative signals provided by loss or gain of interactions by KO and/or KI of glycosyltransferase genes are used to interpret the structural features of the glycans and the glycoconjugates involved. Arguably, we know more about glycosylation pathways and the general roles of glycosyltransferases than the structure of glycans found on specific glycoconjugates and at specific sites in proteins. The genetic engineering design enables attribution of plausible structural features of glycans and the involved types of glycoconjugates, and the availability of appropriate engineered cells enables structural validation and further studies of interactions through the production of targets (Figures 1 and 2).

To test the outcome of the engineering performed, we analyzed a limited set of HEK293 engineered cells (Figure S3). For N-glycans, we compared the profiling of total cell lysates of HEK293^{WT} and isogenic cells engineered to eliminate LacDiNAc (KO *B3GALNT3/4*) or the combination of LacDiNAc, α2-6SA (KO *ST6GAL1*), and multiantennary complex type N-glycans (KO *MGAT3/4A/4B/5*), which, as predicted, resulted in the loss of these glycan features. We further compared these results with site-specific analysis of the N-glycan reporter protein FcγRIIa expressed in the same cells, and this correlated well and confirmed that FcγRIIa faithfully reported the features in question. To evaluate engineering of GalNAc-type O-glycosylation, we stably expressed a secreted MUC1 tandem repeat (TR) reporter construct (Figure S3C), since endo-Asp digestion releases 20-mer TR glycopeptides amenable for O-glycan site and structure analysis by liquid chromatography-tandem mass spectrometry (LC-MS/MS) analysis. The MUC1 reporter expressed in cells with truncated O-glycans (KO *COSMC*) had TRs with 3–5 O-glycosites occupied with HexNAc, while the reporter expressed in cells without the capacity for α2-3SA capping of core1 and core2 synthesis (KO *ST3GAL1/2* and *GCNT1*) produced TRs with 24 O-glycosites with core1 structures (Hassan et al., 2000). To evaluate the GAG biosynthesis capacity, we used disaccharide analysis of total cell lysates. We eliminated GAG biosynthesis entirely (KO *B4GALT7*) or, selectively, biosynthesis of chondroitin/dermatan sulfate (CS/DS) (KO *CHSY1/3*) or heparan sulfate (HS) (KO *EXTL3*) (Figure S5). The KO of *B4GALT7* was in accordance with a classical CHO mutant cell line (Esko et al., 1987) and, further, in agreement with a comprehensive genetic deconstruction of GAG biosynthesis in CHO cells, with a focus on the complex epimerization and sulfation patterns (Chen et al., 2018).

To specifically probe the outcome at the cell surface of the gene engineering performed, we undertook a series of validation studies. We first tested the performance using plant lectins and antibodies with known glycan specificities. Testing N-glycan-specific features with GNL (high and/or paucimannose) and the

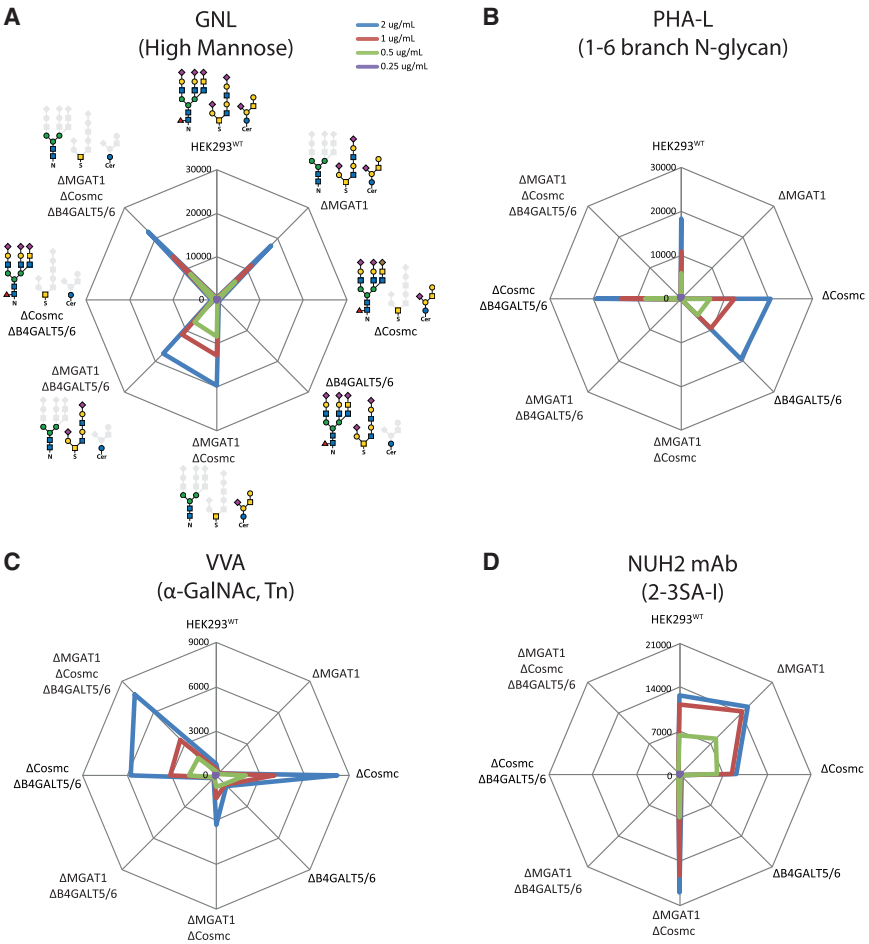

Figure 3. Flow Cytometry Analysis of the Glycoconjugate Sublibrary with Plant Lectins to N-Glycan-Specific Features

(A–C) Sublibrary 1 analyzed with GNL (A), PHA-L (B) and VVA (C) lectins at different concentrations (color coded). Radar charts show mean fluorescence intensities (MFIs), with engineered isogenic HEK293 cells as indicated. The KO engineering (Δ) and predicted display of glycoconjugate structures (solid glycan symbols) are illustrated. Charts represent single experiments, and independent experiments were performed at least three times with similar results.

(D) Sublibrary 1 analyzed with the mAb NUH2. Note minor enhancement in the binding of NUH2 after truncation of N-glycosylation (KO *MGAT1*) and both N- and O-glycosylation (KO *MGAT1/COSMC*), presumably due to the unmasking of glycosphingolipids.

See also Figure S4.

PHA-E and PHA-L lectins (bisecting GlcNAc and tetraantennary N-glycans) on the glycoconjugate sublibrary 1 confirmed that KO of *MGAT1* induced GNL binding and high-Man on the cell surface, while this conversely abrogated PHA labeling and complex-type N-glycans, as predictable (Figures 3A, 3B, and S4A). Similarly, the binding of RCA-1, ECL, and DSL (Galβ1-4GlcNAc; core βGlcNAc) were largely dependent on the capacity for elaborated N-glycosylation (KO *MGAT1*), while capacity for elaborated glycolipid biosynthesis also slightly influenced binding (KO *B4GALT5/6*). Testing GalNAc-type O-glycan-specific features with VVA and GSL-1 (αGalNAc, Tn), as well as Jacalin and MPL (Galβ1-3GalNAc, T; αGalNAc, Tn), revealed a strong induction of binding only when O-glycans were truncated to Tn (KO *COSMC*) (Figures 3C and S4A). The WFL lectin (α/βGalNAc, LacDiNAc and Tn) binding to wild-type (WT) cells was eliminated by truncation of N-glycans (KO *MGAT1*) predicted to be due to the loss of LacDiNAc on N-glycans; while truncation of O-glycans (KO *COSMC*) enhanced binding, presumably due to binding to Tn (Figure S4A). These results all corroborated the predicted outcome of the engineering designs.

To specifically probe glycosphingolipids, we tested the monoclonal antibody (mAb) NUH2 with sperm-immobilizing activity, previously shown to bind α2-3SA-capped symmetric I-branched glycolipids (Nudelman et al., 1989), as an illustrative example for the use of multiple data points from different sublibraries to predict detailed structure information of a binding epitope. NUH2 binding was first tested on the glycoconjugate library 1, and the binding was exclusively dependent on glycolipids (KO *B4GALT5/6*) (Figure 3D), which demonstrated that elaborated lactoseries glycolipids are readily detectable. Testing sublibrary 7 confirmed that NUH2 requires α2-3SA (Figure S4B) but also interestingly demonstrated an absolute requirement for the *ST3GAL6* isoform, suggesting that this isoenzyme has a unique specificity for at least I-branched lactosamine. We confirmed the requirement for the I-branching structure (KO of *GCNT2*) that completely abrogated NUH2 binding. KO and/or KI of *ST3GAL4* did not affect NUH2 binding, showing that only the ST3Gal-VI sialyltransferase can produce this epitope on glycolipids. The mAb 1B2, directed to LacNAc (Young et al., 1981), confirmed the effects of eliminating the α2-3SA and/or α2-6SA sialylation capacities for LacNAc-based substrates (Figure S4C). This also demonstrated that capping of LacNAc in HEK293^{WT} cells is primarily based on α2-3SA, although α2-6 capping is detectable, as demonstrated by SNA lectin binding (Figure 5). We also tested the efficiency of blocking uncapped LacNAc by KI of *ST6GAL1* or *ST3GAL4* in the combinatorial *ST6GAL1/2* and *ST3GAL3/4/6* KO cells, and *ST3GAL4* was slightly more efficient than *ST6GAL1*. These results also corroborated the predicted outcome of the engineering designs and added knowledge of non-redundant functions of the ST3Gal isoenzymes.

Throughout the study, we used live cells for flow cytometry analyses, which requires growing and maintaining the cell libraries in real time. While this clearly is possible for ongoing experiments, we also demonstrated the feasibility of using fixed and frozen cell stocks for subsequent flow cytometry analyses directly after rethawing with lectins and antibodies (Figure S6).

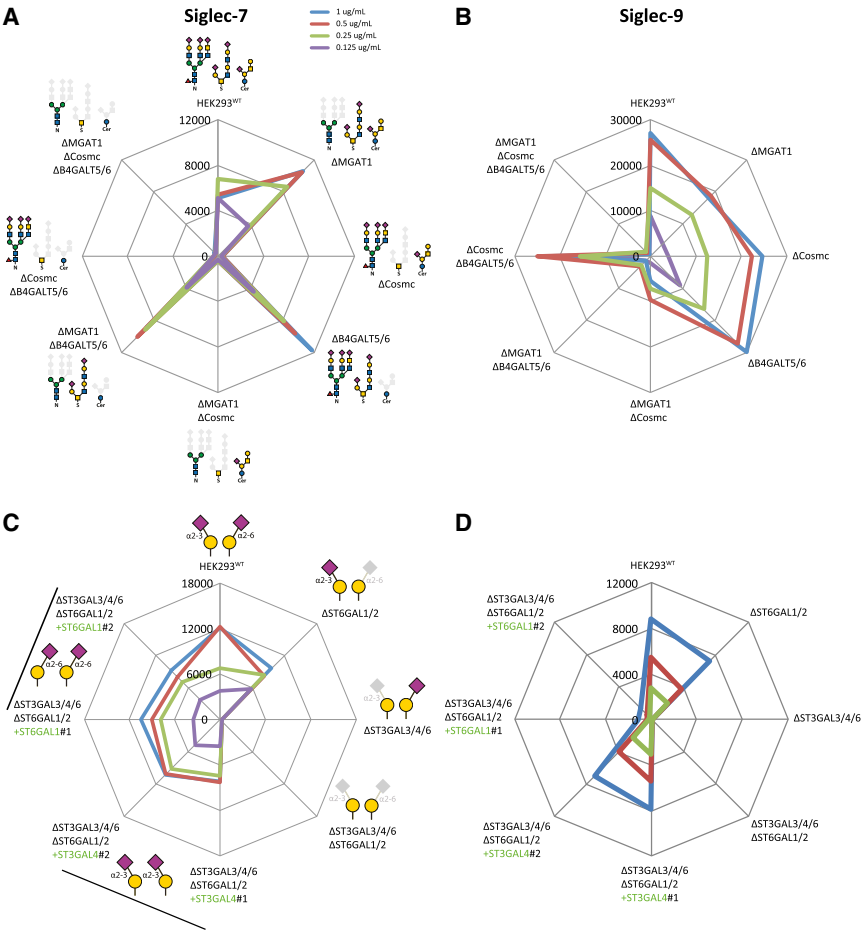

Figure 4. Flow Cytometry Analysis with Siglecs

(A and B) Analysis of glycoconjugate sublibrary 1 with Siglec-7 (A) and -9 (B) at different concentrations. Radar charts indicate MFIs.

(C and D) Analysis of a modified α2-3 or α2-6SA sublibrary 7 with genes introduced by KI indicated in green, and two clones of each KI design were tested (indicated by line and 1 and 2) with Siglec-7 (C) and Siglec-9 (D). We included combinatorial KO of α2-3 and α2-6 sialylation capacities for LacNAc (KO *ST3GAL3/4/6* and *ST6GAL1/2*), with KI of ST3GAL4 or ST6GAL1 to ensure efficient presentation of α2-3 or α2-6SA capping, because KO of *ST3GAL3/4/6* only slightly enhanced binding of SNA, suggesting that ST6GAL1 did not fully compensate for the loss of α2-3 sialylation of LacNAc (see Figure 5A). The charts represent single experiments, and independent experiments were performed at least three times, with similar results.

This strategy obviously enables the distribution of vials or 96-well plates with sublibraries for ease of analysis in cell-binding experiments; however, the cell-based array can be used in many other assay formats where viable cells may be needed.

Applying the Cell-Based Glycan Array for Dissecting Glycan-Binding Specificities

Siglecs

Siglecs are a group of SA-binding immunoglobulin-like lectins with important immunoregulatory functions (Macauley et al., 2014). The specificity of human Siglec-7 is reported to be broad, with binding to α2-8SA-capped sulfated oligosaccharides, gangliosides, and bacterial polysaccharides. Testing sublibrary 1 with Siglec-7 revealed a clear requirement for O-glycans, while sublibrary 7 revealed that elimination of α2-3SA, specifically, on LacNAc destroyed binding, suggesting that Siglec-7 recognizes core2 O-glycans with SA capping (Figures 4A and 4C). Interestingly, re-engineering sialylation capacity through combined KO of α2-3SA and α2-6SA capping on LacNAc or LacDiNAc and the reintroduction of either *ST3GAL4* or *ST6GAL1* reinstated binding. Siglec-7 was shown to bind both α2-3 and α2-6SA, and we predict that core2 O-glycans in HEK293^{WT} primarily are capped by α2-3SA. The effects of α2-8SA were not investigated, but HEK293 cells express a limited number of ST8SIAs.

Human Siglec-9 is reported to bind α2-3SA-capped LacNAc with flexibility of substitutions on the internal HexNAc residue (6-sulfation and α3-fucose) (Yu et al., 2017). Testing sublibrary 1 revealed that Siglec-9 binding was dependent primarily on N-glycans, and sublibrary 7 revealed a strict requirement for α2-3SA on LacNAc (Figures 4B and 4D). Siglec-9 is reported to also bind MUC1 with α2-3SA-capped core1 (Beatson et al., 2016), but we were unable to demonstrate substantial binding to the MUC1 reporter, and studies with printed glycan arrays also showed no or low binding to sialylated core1 (Padler-Karavani et al., 2012; Yu et al., 2017). A recent study demonstrated that the Siglec-7 ligands were sensitive to a mucin-specific protease, while ligands for Siglec-9 were not, which further supports our findings (Malaker et al., 2019).

Influenza Virus HA

The receptor specificity of influenza virus is essential for virus transmission in different species (Paulson and de Vries, 2013). The influenza surface HA binds SA receptors, leading to membrane fusion, while the neuraminidase (NA) cleaves SA from the receptor, enabling release of the virus (Skehel and Wiley, 2000). Extensive studies with different binding assays and printed glycan arrays have established that human pandemic influenza viruses from over a century (1918 [H1N1], 1957 [H2N2], 1968 [H3N2], and 2009 [H1N1]) have a preference for α2-6SA receptors (human type), while HAs from avian viruses have a preference for α2-3SA receptors (avian type) (Paulson and de Vries, 2013; Rillahan and Paulson, 2011). Testing sublibrary 7 with representative HAs, including two of avian origin (Duck/Ukraine/1963 H3 and Vietnam/2004 H5) and two human (Hong Kong/1968 H3 and Texas/2010 H1), recapitulated the selective α2-3/2-6SA receptor specificities (Figure 5A). While the α2-6SA binding lectin SNA reacted weakly with HEK293^{WT} and retained binding after eliminating α2-3SA capping of LacNAc

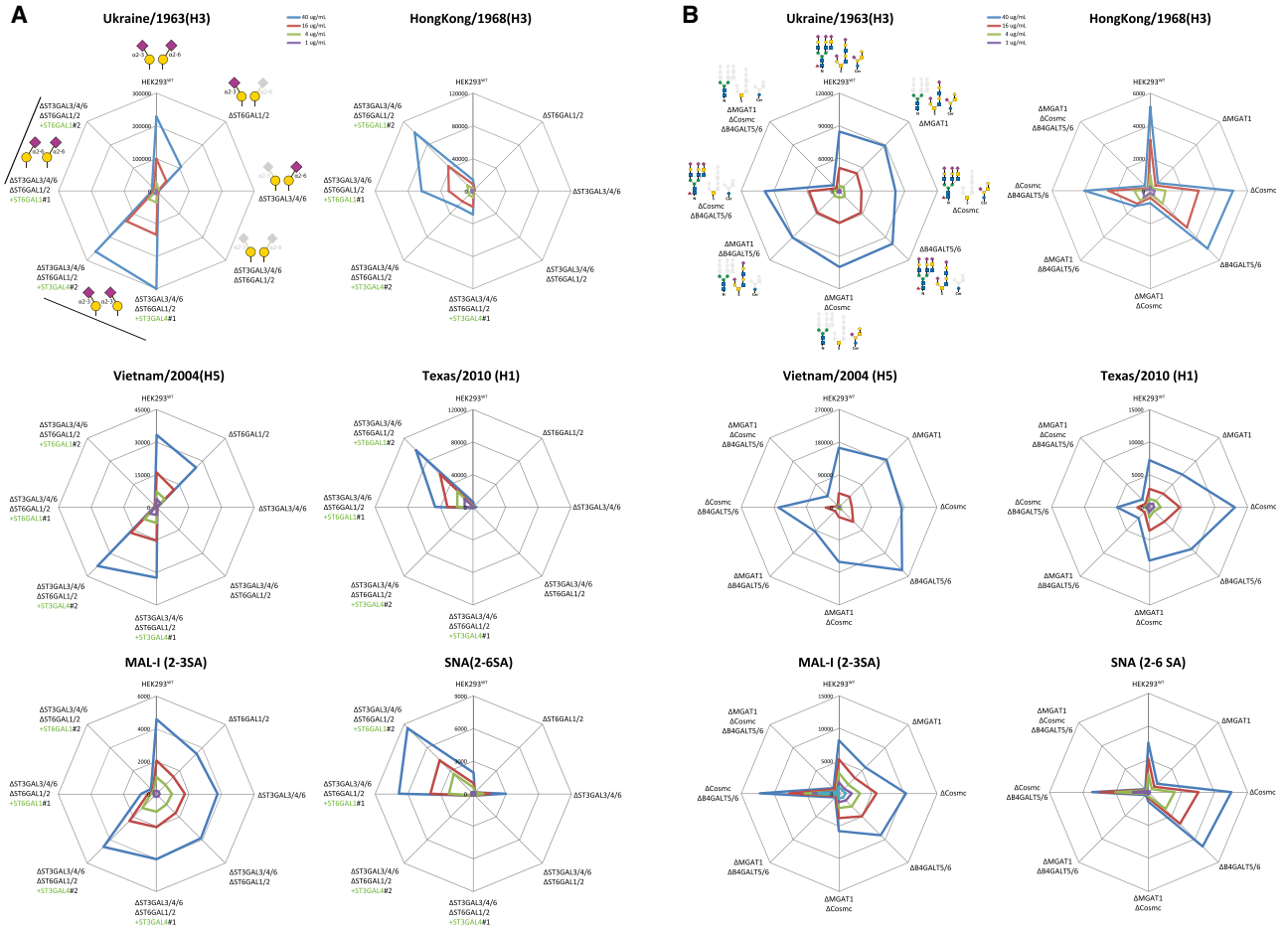

Figure 5. Flow Cytometry Analysis with Influenza HAs

(A) Analysis of modified α2-3 or α2-6SA sublibrary 7 at different concentrations of four HAs and control lectins. Radar charts show MFIs.

(B) Analysis of glycoconjugate sublibrary 1. The charts represent single experiments, and independent experiments were performed at least three times and, when available, with multiple clones, with similar results.

or LacDiNAc (KO *ST3GAL3/4/6*), the two human HAs mainly reacted after KI of *ST6GAL1*, which also induced higher SNA binding. Interestingly, a low but detectable binding of the Hong Kong/1968 H3 to α2-3SA was demonstrated with a KI of *ST3GAL4*, while a simple KO of *ST6GAL1* did not reveal this. This has been predicted based on the close evolutionary relationship with the avian virus, but it has not been possible to demonstrate this previously using printed glycan arrays.

Further testing of glycoconjugates involved in binding revealed that the avian HAs bound equally well to N-glycans, GalNAc-type O-glycans, and glycolipids, and only KO of all three types resulted in abrogation of binding (Figure 5B). Interestingly, the Hong Kong/1968 HA showed strong preferential dependence on N-glycans, resembling the binding pattern of SNA, suggesting that the early HA had preference for N-glycoproteins. In contrast, the later Texas 2010 HA accepted both N-glycans and glycolipids. The α2-3SA binding lectin MAL-I showed strong preference for both N-glycoproteins and glycolipids, while O-glycans alone did not support binding. The ST6Gal-I sialyltransferase is known to transfer to terminal LacNAc core structures on all types of glycoconjugates, but studies have also demonstrated competitive advantages of ST3Gals over ST6Gal-I (Weinstein et al., 1982).

Streptococcal Serine-Rich Adhesins

The serine-rich repeat (SRR) adhesins of commensal and pathogenic Gram-positive bacteria have highly divergent ligand-binding regions and bind to different ligands (Bensing et al., 2016). A group of these adhesins expressed by oral streptococci contains "Siglec-like" binding regions and bind to α2-3SA on the human salivary mucin MUC7 and the platelet membrane glycoprotein 1bα (GP1bα) (Bensing et al., 2016). The binding to MUC7 is believed to be important for natural oral colonization and serendipitous binding to GP1bα for adherence to platelets in the pathogenesis of endocarditis (Deng et al., 2014). The Siglec-like adhesins have shown a preference for α2-3SA on O-glycans (Deng et al., 2014; Bensing et al., 2018), but the selectivity for just a small subset of mucins or mucin-like proteins is not fully understood. We first tested binding to HEK293^{WT} cells

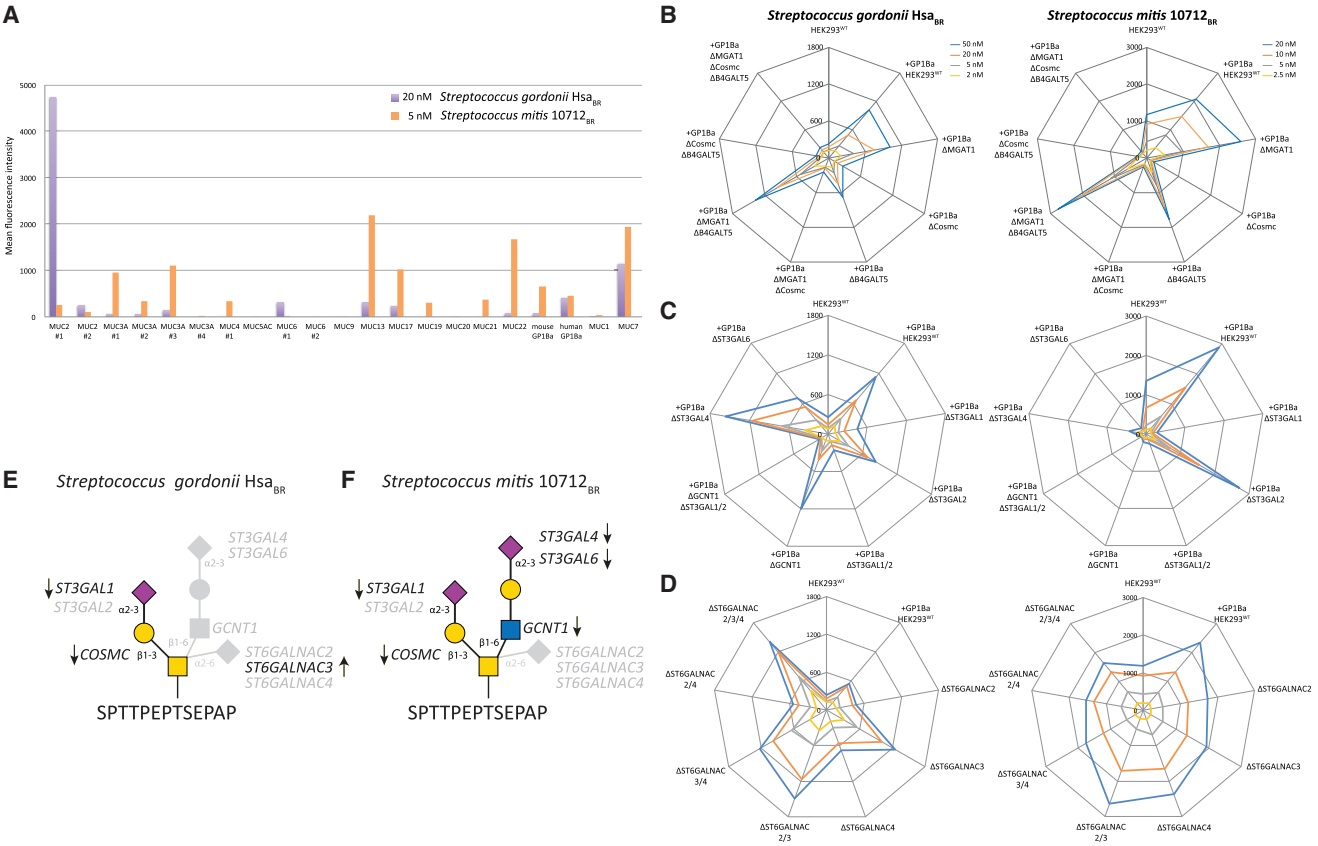

Figure 6. Flow Cytometry Analysis with Streptococcus Adhesins

(A) Analysis of HEK293^{WT} cells transiently expressing 21 human mucin and mucin-like (GP1bα) reporter constructs at one concentration. MFIs were quantified for the cell population positive for the reporter ECFP tag.

(B and C) Analysis of HEK293 cells stably expressing the GP1bα mucin reporter construct with engineering designs from sublibraries 1 (B), 4, and 7 (C), as indicated.

(D) Analysis of sublibrary 8. The charts represent single experiments performed at different concentrations of adhesins, as indicated. Experiments were performed at least three times.

(E and F) Depiction of the distinct O-glycan structures demonstrated to be important for binding of the Hsa$_{BR}$ (E) and 10721$_{BR}$ (F) adhesins, with the positive (arrows) and negative (faded) data points obtained and used for the structural interpretation.

by using the binding regions derived from *Streptococcus mitis* (10712$_{BR}$) and *Streptococcus gordonii* (Hsa$_{BR}$). Reported oligosaccharide ligands for 10712$_{BR}$ include α2-3SA on LacNAc structures (NeuAcα2-3Galβ1-4(Fucα1-3)$^{+/-}$GlcNAc) and, for Hsa$_{BR}$, α2-3SA on LacNAc as well as on Galβ1-3GalNAc found with GalNAc-type O-glycans. Despite the finding that HEK293^{WT} cells display substantial α2-3SA, we found only low binding. We considered the reported selectivity for GP1bα and MUC7 and designed reporter constructs containing the high-density O-glycan regions derived from the stem region of GP1bα and TRs of different mucins (Table S2). We transiently expressed these reporters of mucin domains in HEK293^{WT} and evaluated binding (Figure 6A). Surprisingly, the 10712$_{BR}$ and Hsa$_{BR}$ adhesins showed markedly enhanced but different binding selectivity to cells displaying the mucin reporter constructs. Both adhesins bound cells expressing the GP1bα and MUC7 reporters, but there were striking differences in binding to other mucins; e.g., the only mucin with characterized O-glycan occupancy, MUC1 (Hassan et al., 2000; Müller and Hanisch, 2002), did not support binding by either adhesins. As shown in Figure S3C, the MUC1 reporter clearly displays the uncapped truncated Tn or core1 O-glycans, as predicted from the engineering designs. We, therefore, stably expressed the GP1bα reporter containing the densely O-glycosylated stem region in HEK293^{WT} cells and superimposed the gene engineering for the glycoconjugate sublibrary 1 design (Figures 6B–6D). This modified library demonstrated that Hsa$_{BR}$ and 10712$_{BR}$ binding was selectively abolished by the loss of elongated O-glycans (KO *COSMC*). Applying the O-glycan branching sublibrary 4 further interestingly showed that 10712$_{BR}$ binding was also abolished by the loss of core2 O-glycans (KO *GCNT1*), whereas Hsa$_{BR}$ binding was unaffected. Thus, Hsa$_{BR}$ binding does not require core2, and it may not be impeded by a core2 branch (Bensing et al., 2018). Further analysis of sialyltransferases with sublibrary 7 revealed that Hsa$_{BR}$ binding was abrogated by the loss of α2-3SA on core1 O-glycans (KO *ST3GAL1/2*) and was specifically activated by loss of α2-6SA on core1 (KO *ST6GALNAC3*). These results indicate that the minimum binding epitope of Hsa$_{BR}$ is a

monosialylated core1 O-glycan (NeuAcα2-3Galβ1-3GalNAcα1-O-Ser/Thr), while the disialylated structure (NeuAcα2-3Galβ1-3(NeuAcα2-6)GalNAcα1-O-Ser/Thr) is not (Figure 6E). 10712_{BR} binding was abolished by loss of α2-3SA on core1 (KO *ST3GAL1*) as well as on LacNAc (KO *ST3GAL4/6*), and the preferred binding epitope is, therefore, predicted to be a complex core2 O-glycan with two terminal α2-3SA residues (NeuAcα2-3Galβ1-3(NeuAcα2-3Galβ1-4GlcNAcβ1-6)GalNAcα1-O-Ser/Thr) (Figure 6F). It is important to note that the current library does not include α1-3Fuc residues. The different effects of KO of *ST3GAL1/2* and *ST6GALNAC2/3/4* for binding of the adhesins indicate interesting fine specificities of these isoenzymes that need further exploration.

Collectively, these results suggest that the Siglec-like adhesins recognize specific O-glycan structures in ways influenced by their presentation on the protein or mucin backbone. While further studies are needed, the likely explanation for this is the recognition of clustered patches or patterns of multiple O-glycans. Simple multivalent presentation of O-glycans does not seem to rule, since all the reporter constructs studied are predicted to present multiple closely spaced O-glycans. Mucin TRs and mucin-like domains such as the stem region of GP1bα are characterized by being densely decorated with O-glycans, and the positions and patterns of the O-glycan decoration are determined by the peptide sequence (distribution of Ser/Thr residues) and the specificities of the available polypeptide GalNAc-transferases (*GALNT1-20*) that control initiation of O-glycosylation (Bennett et al., 2012). Analysis of the sequences used for the reporter constructs derived from the mucin TRs and GP1bα did not reveal simple common sequence motifs shared among those providing binding for the Siglec-like adhesins; thus, the data do not enable us to define the recognition motifs in further detail. Recognition of "clustered saccharide patches" orchestrated by positions, spacing, and direct interactions of multiple glycans in a protein was earlier proposed to provide expanded binding specificities and high-affinity interactions, and evidence in support of this has been found with all types of glycoconjugates (Cohen and Varki, 2014; Varki, 1994).

DISCUSSION

Here, we developed a sustainable platform for cell-based display of a substantial part of the human glycome that enables wide surveying of the informational content of human glycans. Use of the cell-based glycan display is fundamentally different than use of printed glycan arrays in that the primary readout is the consequence of the loss or gain of glycosyltransferase genes that are used to predict structural glycan features. Printed glycan arrays provide direct information of glycan haptens involved in interactions, while the cell-based array provides comprehensive knowledge of genes regulating the expression of glycan features. By organizing sublibraries designed to independently query the glycoconjugate status, features specific for individual glycosylation pathways and features more commonly found on glycoconjugates, we reached manageable-sized cell libraries that can be used broadly by the community. We illustrate the utility and discovery potential of the cell-based platform by applying it to dissect the sialic-acid-dependent adhesion of influenza HAs and streptococcal Siglec-like adhesins. These studies fully recapitulated previous results, provided further structural refinements of the binding motifs of glycan structures, and led to the discovery of the importance of the glycoconjugate context for binding. The cell-based array reports the genetic and biosynthetic regulation of glycan binding motifs, and the strategy inherently generates engineered cells that can be used for the production of reporter glycoproteins and further structural analysis, validation, and other biological assays. The current design of the array covers the human glycome quite widely, but continuous efforts are needed to custom-design sublibraries (connectivities) for specific applications, which are facilitated by the atlas of glycosylation pathways and the library of validated gRNA-targeting constructs (Narimatsu et al., 2018).

Printed glycan arrays have transformed the field of glycosciences and served as essential tools for exploring the interactome of glycans and proteins (Rillahan and Paulson, 2011); however, studies have also resulted in the emergence of an interesting conundrum in explaining the diversity of pathogen interactions and their host tropism in nature (Cohen and Varki, 2014; Cummings, 2009). Results from printed glycan arrays indicate that relatively few distinct glycan motifs serve as common ligands for many microbial adhesins and glycan-binding proteins (Cummings, 2009). The core structural motifs recognized, typically only 3–5 monosaccharides, are even more limited, since glycans are built on common scaffolds with units such as LacNAc (Blixt et al., 2004; Cummings, 2009). Many host-pathogen interactions identified involve terminal SA residues on common structural motifs, and while the glycosidic linkages, the underlying core structures, and numerous modifications of SAs (Varki et al., 2015b), do vary to a degree, the overall structural permutations are still somewhat limited. It therefore seems likely that additional features, such as the context of these binding motifs with respect to the glycoconjugate carrying the glycans, interactions with adjacent glycans, and their overall presentation at the cell membrane may further enhance specificity. Traditional printed glycan arrays display different oligosaccharides without the context of the overall glycoconjugate and often in high densities, disproportionate to those normally found at the cell surface (Blixt et al., 2004), and the immobilization strategies may also affect lectin binding results (Padler-Karavani et al., 2012).

The cell-based array format can overcome some of these issues and provide further refinements of complex binding motifs, and this was clearly demonstrated with the streptococcal adhesins, where we uncovered a higher order diversity in binding to specific O-glycans presented on different mucin peptide TR backbones (Figure 6). Mucins are ideally designed to present O-glycans in high densities and distinct patterns with their diverse TR sequences (Hollingsworth and Swanson, 2004), and the decoration with O-glycans is differentially regulated by the many polypeptide GalNAc transferases that enables cell-specific glycosylation patterns (Bennett et al., 2012). The complex interplay of positions and structures of O-glycans on distinct mucin TRs is not addressable by traditional printed glycan arrays, and structural analysis of mucin TRs is largely impossible.

The results obtained here with the cell-based array strongly suggest that the informational content of mucin TRs is far greater than expected and, essentially, yet unexplored. Mucins are suggested to be poorly conserved in evolution because of high divergence in their TRs; however, an alternative interpretation relevant to our findings here may be that divergence in TRs has evolved under selective pressure in response to recognition of specific patterns and clusters of O-glycans. The panel of human mucin TR reporters and the cell-based glycan display platform now allows for wider studies of how clusters and patterns of O-glycans on mucins are recognized by microbial adhesins.

Analysis of influenza HAs with the cell-based array also pointed to new insights into the difference in SA receptors for avian and human influenza HAs (Figure 5). The α2-3SA binding specificity of avian HAs and α2-6SA specificity of human HAs were clearly recapitulated. However, importantly, low binding to α2-3SA was seen with the Hong Kong/1968 (H3) HA, consistent with the fact that this virus is derived from the avian (duck) Ukraine/1963 (H3) precursor and had just entered the human population (Ha et al., 2003). The analysis also alluded to differences in the types of glycoconjugates recognized by avian and human HAs, with avian HAs showing binding to all three of the major α2-3SA-carrying glycoconjugates and human HAs showing variable dependence on the expression of α2-6SA on N-glycoproteins and glycolipids. Further dissection combining the sialylation and glycoconjugate sublibraries can now be performed to explore these interesting findings in greater detail.

In summary, the cell-based array differentially displays the human glycome in a natural glycoconjugate and cell-surface context and is likely to generate a new and deeper understanding of the many biological roles of the glycome. Importantly, the cell-based array provides specific information of regulatory genes that can be directly used to further explore and validate findings by any cell biologist without detailed insight into glycosciences and access to advanced glycan analytics. These studies should be facilitated by the classification and overview of glycosylation pathways (Figure 1) and the library of validated CRISPR/Cas9 gRNA targeting constructs for all human glycosyltransferase genes (Narimatsu et al., 2018). Limitations with the cell-based array design are the current size of the cell libraries, connectivity between sublibraries, and glycan features still missing, but these can be improved with future expansion. The array can be used when substantial changes in cell binding and/or other assay readouts are obtainable in response to a gene KO and/or KI design, but it is important to consider that the intensity of signals may vary due to overlapping functions and competition of enzymes, which may not always yet be predictable from the presented pathways. It is especially important to consider the potential requirement for specific proteins not expressed in HEK293 to obtain optimal and biologically relevant signals. Finally, the interpretation of structural glycan features involved in observed interactions relies on predictions based on the current understanding of glycosylation pathways, and it is important to consider unpredictable outcomes and use data points from multiple logical biosynthetic steps to strengthen predictions. The array will be made broadly available to the community, and we hope that the simple cellular platform and matrix for interpretation provided will help engage use beyond the glycoscience field.

STAR★METHODS

Detailed methods are provided in the online version of this paper and include the following:

- KEY RESOURCES TABLE
- CONTACT FOR REAGENT AND RESOURCE SHARING
- METHOD DETAILS
  - Cell Culture
  - Gene constructs and other reagents
  - Transcriptome analysis in HEK293 cell line
  - CRISPR/Cas9 targeted KO in HEK293 cells
  - ZFN-mediated KI in HEK293 cells
  - Stable expression of the GP1bα reporter in HEK293
  - Human mucin reporter constructs
  - Cell binding assays
  - Production of N- and O-glycosylation reporter proteins
  - Sample preparation for site-specific N-glycopeptide analysis
  - Sample preparation for total cell lysate N-glycan analysis
  - Sample preparation for O-glycopeptide analysis
  - Mass Spectrometry
  - Data Analysis
  - Disaccharide analysis of GAGs
- DATA AND SOFTWARE AVAILABILITY

SUPPLEMENTAL INFORMATION

Supplemental Information can be found online at https://doi.org/10.1016/j.molcel.2019.05.017.

ACKNOWLEDGMENTS

This work was supported by the Lundbeck Foundation, the Novo Nordisk Foundation, Kirsten og Freddy Johansens Fond, A.P. Møller Fonden, Læge Sophus Carl Emil Friis og hustru Olga Doris Friis' Legat, the European Commission (GlycoImaging H2020-MSCA-ITN-721297 and BioCapture H2020-MSCA-ITN-722171), the Danish National Research Foundation (DNRF107), the NIH (AI114730, R01AI41513, R01AI106987, and U01OD024857), and the Kuang Hua Educational Foundation.

AUTHOR CONTRIBUTIONS

Y.N. and H.C. conceived and designed the study; Y.-H.C., H.J.J., R.N., R.K., J.V.C., L.S., Z.Y., K.T.S., C.S., S.F., U.M., L.H., E.P.B., S.Y.V., and Z.Y. contributed with experimental data and interpretation; B.A.B., P.M.S., and A.V. contributed to the streptococcal adhesin studies; A.J.T. and J.C.P. contributed to the influenza HA studies; C.B. and G.J.A. contributed to the Siglec studies; Y.N. and H.C wrote the manuscript; and all authors edited and approved the final version.

DECLARATION OF INTERESTS

The University of Copenhagen has filed a patent application on the cell-based display platform. GlycoDisplay Aps, Copenhagen, Denmark, has obtained a license to the field of the patent application. Y.N., Z.Y., E.P.B., and H.C. are cofounders of GlycoDisplay Aps and hold ownerships in the company and served as unpaid consultants.

Received: August 10, 2018
Revised: February 8, 2019
Accepted: May 10, 2019
Published: July 25, 2019

REFERENCES

Beatson, R., Tajadura-Ortega, V., Achkova, D., Picco, G., Tsourouktsoglou, T.D., Klausing, S., Hillier, M., Maher, J., Noll, T., Crocker, P.R., et al. (2016). The mucin MUC1 modulates the tumor immunological microenvironment through engagement of the lectin Siglec-9. Nat. Immunol. *17*, 1273–1281.

Bennett, E.P., Mandel, U., Clausen, H., Gerken, T.A., Fritz, T.A., and Tabak, L.A. (2012). Control of mucin-type O-glycosylation: a classification of the polypeptide GalNAc-transferase gene family. Glycobiology *22*, 736–756.

Bensing, B.A., Khedri, Z., Deng, L., Yu, H., Prakobphol, A., Fisher, S.J., Chen, X., Iverson, T.M., Varki, A., and Sullam, P.M. (2016). Novel aspects of sialoglycan recognition by the Siglec-like domains of streptococcal SRR glycoproteins. Glycobiology *26*, 1222–1234.

Bensing, B.A., Li, Q., Park, D., Lebrilla, C.B., and Sullam, P.M. (2018). Streptococcal Siglec-like adhesins recognize different subsets of human plasma glycoproteins: implications for infective endocarditis. Glycobiology *28*, 601–611.

Blixt, O., Head, S., Mondala, T., Scanlan, C., Huflejt, M.E., Alvarez, R., Bryan, M.C., Fazio, F., Calarese, D., Stevens, J., et al. (2004). Printed covalent glycan array for ligand profiling of diverse glycan binding proteins. Proc. Natl. Acad. Sci. USA *101*, 17033–17038.

Chen, Y.-H., Narimatsu, Y., Clausen, T.M., Gomes, C., Karlsson, R., Steentoft, C., Spliid, C.B., Gustavsson, T., Salanti, A., Persson, A., et al. (2018). The GAGOme: a cell-based library of displayed glycosaminoglycans. Nat. Methods *15*, 881–888.

Cohen, M., and Varki, A. (2014). Modulation of glycan recognition by clustered saccharide patches. Int. Rev. Cell Mol. Biol. *308*, 75–125.

Conzelmann, A., and Kornfeld, S. (1984). Beta-linked N-acetylgalactosamine residues present at the nonreducing termini of O-linked oligosaccharides of a cloned murine cytotoxic T lymphocyte line are absent in a Vicia villosa lectin-resistant mutant cell line. J. Biol. Chem. *259*, 12528–12535.

Cummings, R.D. (2009). The repertoire of glycan determinants in the human glycome. Mol. Biosyst. *5*, 1087–1104.

Deng, L., Bensing, B.A., Thamadilok, S., Yu, H., Lau, K., Chen, X., Ruhl, S., Sullam, P.M., and Varki, A. (2014). Oral streptococci utilize a Siglec-like domain of serine-rich repeat adhesins to preferentially target platelet sialoglycans in human blood. PLoS Pathog. *10*, e1004540.

Esko, J.D., Weinke, J.L., Taylor, W.H., Ekborg, G., Rodén, L., Anantharamaiah, G., and Gawish, A. (1987). Inhibition of chondroitin and heparan sulfate biosynthesis in Chinese hamster ovary cell mutants defective in galactosyltransferase I. J. Biol. Chem. *262*, 12189–12195.

Fujitani, N., Furukawa, J., Araki, K., Fujioka, T., Takegawa, Y., Piao, J., Nishioka, T., Tamura, T., Nikaido, T., Ito, M., et al. (2013). Total cellular glycomics allows characterizing cells and streamlining the discovery process for cellular biomarkers. Proc. Natl. Acad. Sci. USA *110*, 2105–2110.

Fukui, S., Feizi, T., Galustian, C., Lawson, A.M., and Chai, W. (2002). Oligosaccharide microarrays for high-throughput detection and specificity assignments of carbohydrate-protein interactions. Nat. Biotechnol. *20*, 1011–1017.

Ha, Y., Stevens, D.J., Skehel, J.J., and Wiley, D.C. (2003). X-ray structure of the hemagglutinin of a potential H3 avian progenitor of the 1968 Hong Kong pandemic influenza virus. Virology *309*, 209–218.

Hassan, H., Reis, C.A., Bennett, E.P., Mirgorodskaya, E., Roepstorff, P., Hollingsworth, M.A., Burchell, J., Taylor-Papadimitriou, J., and Clausen, H. (2000). The lectin domain of UDP-N-acetyl-D-galactosamine: polypeptide N-acetylgalactosaminyltransferase-T4 directs its glycopeptide specificities. J. Biol. Chem. *275*, 38197–38205.

Hollingsworth, M.A., and Swanson, B.J. (2004). Mucins in cancer: protection and control of the cell surface. Nat. Rev. Cancer *4*, 45–60.

Jae, L.T., Raaben, M., Riemersma, M., van Beusekom, E., Blomen, V.A., Velds, A., Kerkhoven, R.M., Carette, J.E., Topaloglu, H., Meinecke, P., et al. (2013). Deciphering the glycosylome of dystroglycanopathies using haploid screens for lassa virus entry. Science *340*, 479–483.

Joshi, H.J., Hansen, L., Narimatsu, Y., Freeze, H.H., Henrissat, B., Bennett, E., Wandall, H.H., Clausen, H., and Schjoldager, K.T. (2018a). Glycosyltransferase genes that cause monogenic congenital disorders of glycosylation are distinct from glycosyltransferase genes associated with complex diseases. Glycobiology *28*, 284–294.

Joshi, H.J., Narimatsu, Y., Schjoldager, K.T., Tytgat, H.L.P., Aebi, M., Clausen, H., and Halim, A. (2018b). SnapShot: O-Glycosylation Pathways across Kingdoms. Cell *172*, 632–632.e632.

Kingsley, D.M., Kozarsky, K.F., Hobbie, L., and Krieger, M. (1986). Reversible defects in O-linked glycosylation and LDL receptor expression in a UDP-Gal/UDP-GalNAc 4-epimerase deficient mutant. Cell *44*, 749–759.

Lavrsen, K., Dabelsteen, S., Vakhrushev, S.Y., Levann, A.M.R., Haue, A.D., Dylander, A., Mandel, U., Hansen, L., Frödin, M., Bennett, E.P., and Wandall, H.H. (2018). *De novo* expression of human polypeptide *N*-acetylgalactosaminyltransferase 6 (GalNAc-T6) in colon adenocarcinoma inhibits the differentiation of colonic epithelium. J. Biol. Chem. *293*, 1298–1314.

Lonowski, L.A., Narimatsu, Y., Riaz, A., Delay, C.E., Yang, Z., Niola, F., Duda, K., Ober, E.A., Clausen, H., Wandall, H.H., et al. (2017). Genome editing using FACS enrichment of nuclease-expressing cells and indel detection by amplicon analysis. Nat. Protoc. *12*, 581–603.

Lowe, J.B., and Marth, J.D. (2003). A genetic approach to mammalian glycan function. Annu. Rev. Biochem. *72*, 643–691.

Macauley, M.S., Crocker, P.R., and Paulson, J.C. (2014). Siglec-mediated regulation of immune cell function in disease. Nat. Rev. Immunol. *14*, 653–666.

Malaker, S.A., Pedram, K., Ferracane, M.J., Bensing, B.A., Krishnan, V., Pett, C., Yu, J., Woods, E.C., Kramer, J.R., Westerlind, U., et al. (2019). The mucin-selective protease StcE enables molecular and functional analysis of human cancer-associated mucins. Proc. Natl. Acad. Sci. USA *116*, 7278–7287.

Müller, S., and Hanisch, F.G. (2002). Recombinant MUC1 probe authentically reflects cell-specific O-glycosylation profiles of endogenous breast cancer mucin. High density and prevalent core 2-based glycosylation. J. Biol. Chem. *277*, 26103–26112.

Narimatsu, Y., Joshi, H.J., Yang, Z., Gomes, C., Chen, Y.H., Lorenzetti, F.C., Furukawa, S., Schjoldager, K.T., Hansen, L., Clausen, H., et al. (2018). A validated gRNA library for CRISPR/Cas9 targeting of the human glycosyltransferase genome. Glycobiology *28*, 295–305.

Ng, B.G., and Freeze, H.H. (2018). Perspectives on glycosylation and Its congenital disorders. Trends Genet. *34*, 466–476.

Nudelman, E.D., Mandel, U., Levery, S.B., Kaizu, T., and Hakomori, S. (1989). A series of disialogangliosides with binary 2→3 sialosyllactosamine structure, defined by monoclonal antibody NUH2, are oncodevelopmentally regulated antigens. J. Biol. Chem. *264*, 18719–18725.

Padler-Karavani, V., Song, X., Yu, H., Hurtado-Ziola, N., Huang, S., Muthana, S., Chokhawala, H.A., Cheng, J., Verhagen, A., Langereis, M.A., et al. (2012). Cross-comparison of protein recognition of sialic acid diversity on two novel sialoglycan microarrays. J. Biol. Chem. *287*, 22593–22608.

Palma, A.S., Feizi, T., Childs, R.A., Chai, W., and Liu, Y. (2014). The neoglycolipid (NGL)-based oligosaccharide microarray system poised to decipher the meta-glycome. Curr. Opin. Chem. Biol. *18*, 87–94.

Patnaik, S.K., and Stanley, P. (2006). Lectin-resistant CHO glycosylation mutants. Methods Enzymol. *416*, 159–182.

Paulson, J.C., and de Vries, R.P. (2013). H5N1 receptor specificity as a factor in pandemic risk. Virus Res. *178*, 99–113.

Peng, W., de Vries, R.P., Grant, O.C., Thompson, A.J., McBride, R., Tsogtbaatar, B., Lee, P.S., Razi, N., Wilson, I.A., Woods, R.J., and Paulson, J.C. (2017). Recent H3N2 viruses have evolved specificity for extended, branched human-type receptors, conferring potential for increased avidity. Cell Host Microbe *21*, 23–34.

Pinto, R., Hansen, L., Hintze, J., Almeida, R., Larsen, S., Coskun, M., Davidsen, J., Mitchelmore, C., David, L., Troelsen, J.T., and Bennett, E.P. (2017). Precise integration of inducible transcriptional elements (PrIITE) enables absolute control of gene expression. Nucleic Acids Res. *45*, e123.

Puvirajesinghe, T.M., and Turnbull, J.E. (2016). Glycoarray technologies: deciphering interactions from proteins to live cell responses. Microarrays (Basel) *5*, E3.

Rappsilber, J., Mann, M., and Ishihama, Y. (2007). Protocol for micro-purification, enrichment, pre-fractionation and storage of peptides for proteomics using StageTips. Nat. Protoc. *2*, 1896–1906.

Rillahan, C.D., and Paulson, J.C. (2011). Glycan microarrays for decoding the glycome. Annu. Rev. Biochem. *80*, 797–823.

Schjoldager, K.T., Joshi, H.J., Kong, Y., Goth, C.K., King, S.L., Wandall, H.H., Bennett, E.P., Vakhrushev, S.Y., and Clausen, H. (2015). Deconstruction of O-glycosylation—GalNAc-T isoforms direct distinct subsets of the O-glycoproteome. EMBO Rep. *16*, 1713–1722.

Schulz, M.A., Tian, W., Mao, Y., Van Coillie, J., Sun, L., Larsen, J.S., Chen, Y.H., Kristensen, C., Vakhrushev, S.Y., Clausen, H., and Yang, Z. (2018). Glycoengineering design options for IgG1 in CHO cells using precise gene editing. Glycobiology *28*, 542–549.

Skehel, J.J., and Wiley, D.C. (2000). Receptor binding and membrane fusion in virus entry: the influenza hemagglutinin. Annu. Rev. Biochem. *69*, 531–569.

Steentoft, C., Vakhrushev, S.Y., Vester-Christensen, M.B., Schjoldager, K.T., Kong, Y., Bennett, E.P., Mandel, U., Wandall, H., Levery, S.B., and Clausen, H. (2011). Mining the O-glycoproteome using zinc-finger nuclease-glycoengineered SimpleCell lines. Nat. Methods *8*, 977–982.

Steentoft, C., Bennett, E.P., Schjoldager, K.T., Vakhrushev, S.Y., Wandall, H.H., and Clausen, H. (2014). Precision genome editing: a small revolution for glycobiology. Glycobiology *24*, 663–680.

Stolfa, G., Mondal, N., Zhu, Y., Yu, X., Buffone, A., Jr., and Neelamegham, S. (2016). Using CRISPR-Cas9 to quantify the contributions of O-glycans, N-glycans and glycosphingolipids to human leukocyte-endothelium adhesion. Sci. Rep. *6*, 30392.

Termini, J.M., Silver, Z.A., Connor, B., Antonopoulos, A., Haslam, S.M., Dell, A., and Desrosiers, R.C. (2017). HEK293T cell lines defective for O-linked glycosylation. PLoS ONE *12*, e0179949.

Thomas, P., and Smart, T.G. (2005). HEK293 cell line: a vehicle for the expression of recombinant proteins. J. Pharmacol. Toxicol. Methods *51*, 187–200.

Vakhrushev, S.Y., Dadimov, D., and Peter-Katalinić, J. (2009). Software platform for high-throughput glycomics. Anal. Chem. *81*, 3252–3260.

Varki, A. (1994). Selectin ligands. Proc. Natl. Acad. Sci. USA *91*, 7390–7397.

Varki, A., Cummings, R.D., Aebi, M., Packer, N.H., Seeberger, P.H., Esko, J.D., Stanley, P., Hart, G., Darvill, A., Kinoshita, T., et al. (2015a). Symbol nomenclature for graphical representations of glycans. Glycobiology *25*, 1323–1324.

Varki, A., Schnaar, R.L., and Schauer, R. (2015b). Sialic acids and other nonulosonic acids. In Essentials of Glycobiology, Third ed, A. Varki, R.D. Cummings, J.D. Esko, P. Stanley, G.W. Hart, M. Aebi, A.G. Darvill, T. Kinoshita, N.H. Packer, and J.H. Prestegard, et al., eds. (Cold Spring Harbor Laboratory Press), pp. 179–195.

Wang, Z., Chinoy, Z.S., Ambre, S.G., Peng, W., McBride, R., de Vries, R.P., Glushka, J., Paulson, J.C., and Boons, G.J. (2013). A general strategy for the chemoenzymatic synthesis of asymmetrically branched N-glycans. Science *341*, 379–383.

Wasik, B.R., Barnard, K.N., Ossiboff, R.J., Khedri, Z., Feng, K.H., Yu, H., Chen, X., Perez, D.R., Varki, A., and Parrish, C.R. (2017). Distribution of O-acetylated sialic acids among target host tissues for influenza virus. mSphere *2*, e00379-16.

Weinstein, J., de Souza-e-Silva, U., and Paulson, J.C. (1982). Sialylation of glycoprotein oligosaccharides N-linked to asparagine. Enzymatic characterization of a Gal beta 1 to 3(4)GlcNAc alpha 2 to 3 sialyltransferase and a Gal beta 1 to 4GlcNAc alpha 2 to 6 sialyltransferase from rat liver. J. Biol. Chem. *257*, 13845–13853.

Yang, X., Tao, S., Orlando, R., Brockhausen, I., and Kan, F.W. (2012). Structures and biosynthesis of the N- and O-glycans of recombinant human oviduct-specific glycoprotein expressed in human embryonic kidney cells. Carbohydr. Res. *358*, 47–55.

Yang, Z., Steentoft, C., Hauge, C., Hansen, L., Thomsen, A.L., Niola, F., Vester-Christensen, M.B., Frödin, M., Clausen, H., Wandall, H.H., and Bennett, E.P. (2015a). Fast and sensitive detection of indels induced by precise gene targeting. Nucleic Acids Res. *43*, e59.

Yang, Z., Wang, S., Halim, A., Schulz, M.A., Frodin, M., Rahman, S.H., Vester-Christensen, M.B., Behrens, C., Kristensen, C., Vakhrushev, S.Y., et al. (2015b). Engineered CHO cells for production of diverse, homogeneous glycoproteins. Nat. Biotechnol. *33*, 842–844.

Young, W.W., Jr., Portoukalian, J., and Hakomori, S. (1981). Two monoclonal anticarbohydrate antibodies directed to glycosphingolipids with a lacto-N-glycosyl type II chain. J. Biol. Chem. *256*, 10967–10972.

Yu, H., Gonzalez-Gil, A., Wei, Y., Fernandes, S.M., Porell, R.N., Vajn, K., Paulson, J.C., Nycholat, C.M., and Schnaar, R.L. (2017). Siglec-8 and Siglec-9 binding specificities and endogenous airway ligand distributions and properties. Glycobiology *27*, 657–668.

STAR★METHODS

KEY RESOURCES TABLE

REAGENT or RESOURCE	SOURCE	IDENTIFIER
Antibodies		
Mouse anti 6xHis tag	Thermo	Cat#MA1-21315; RRID:AB_557403
Goat anti-mouse IgG (H+L), Alexa Fluor™ 647	Invitrogen	Cat#A-21235; RRID:AB_2535804
Streptavidin, Alexa Fluor™ 488 conjugate	Invitrogen	Cat#S32354; RRID:AB_231583
Goat anti-Human IgG (H+L), Alexa Fluor™ 647	Invitrogen	Cat#A-21445; RRID:AB_2535862
GST tag polyclonal antibody	Invitrogen	Cat#71-7500; RRID:AB_2533994
Goat anti-Rabbit IgG (H+L), Alexa Flouor™ 647	Invitrogen	CatA-21245; RRID:AB_2535813
NUH2 antibody	Nudelman et al., 1989	N/A
1B2 antibody	Young et al., 1981	N/A
Biological Samples		
Chemicals, Peptides, and Recombinant Proteins		
Influenza hemagglutinins	Paulson and de Vries, 2013	N/A
Streptococcus	Bensing et al., 2016	N/A
Recombinant Human Siglec-7/CD328 Fc Chimera	R&D systems	Cat#1138-SL
Recombinant Human Siglec-9 Fc Chimera	R&D systems	Cat#1139-SL
Biotinylated Lens Culinaris Agglutinin (LCA)	Vector Laboratories	Cat#B-1045; RRID:AB_2336552
Biotinylated Concanavalin A (Con A)	Vector Laboratories	Cat#B-1005; RRID:AB_2313506
Biotinylated Jacalin	Vector Laboratories	Cat#B-1155; RRID:AB_2336541
Biotinylated Galanthus Nivalis Lectin (GNL)	Vector Laboratories	Cat#B-1245; RRID:AB_2336469
Biotinylated Maclura Pomifera Lectin (MPL)	Vector Laboratories	Cat#B-1345; RRID:AB_2336571
Biotinylated Vicia Villosa Lectin (VVL, VVA)	Vector Laboratories	Cat#B-1235; RRID:AB_2336855
Biotinylated Griffonia Simplicifolia Lectin I (GSL I, BSL I)	Vector Laboratories	Cat#B-1105; RRID:AB_2336489
Biotinylated Datura Stramonium Lectin (DSL)	Vector Laboratories	Cat#B-1185; RRID:AB_2336384
Biotinylated Ricinus Communis Agglutinin I (RCA I, RCA120)	Vector Laboratories	Cat#B-1085; RRID:AB_2336707
Biotinylated Erythrina Cristagalli Lectin (ECL, ECA)	Vector Laboratories	Cat#B-1145; RRID:AB_2336436
Biotinylated Phaseolus Vulgaris Erythroagglutinin(PHA-E)	Vector Laboratories	Cat#B-1125; RRID:AB_2336650
Biotinylated Phaseolus Vulgaris Leucoagglutinin(PHA-L)	Vector Laboratories	Cat#B-1115; RRID:AB_2336654
Biotinylated Wisteria Floribunda Lectin (WFA, WFL)	Vector Laboratories	Cat#B-1355; RRID:AB_2336874
Biotinylated Maackia Amurensis Lectin I (MAL I)	Vector Laboratories	Cat#B-1315; RRID:AB_2336566
Biotinylated Sambucus Nigra Lectin (SNA, EBL)	Vector Laboratories	Cat#B-1305; RRID:AB_2336718
DMEM-high glucose	Sigma	Cat#D-5796
Fetal Bovine Serum (heat activated)	Sigma	Cat#F9665
Glutamax	GIBCO	Cat#35050061
TrypLE™ Express Enzyme (1X), phenol red	GIBCO	Cat#12605028
F17 medium	Invitrogen	Cat#A13835-01
Kolliphor P188	Sigma	Cat#K4894-500 g
Polyethylenimine (linear, 25 kDa)	Polysciences	Cat#23966
Ni-NTA Agarose	QIAGEN	Cat#30210
Jupiter® 5 μm C4 300 Å, LC Column 250 × 4.6 mm	Phenomenex	Cat#00G-4167-E0
Deposited Data		
Experimental Models: Cell Lines		
Human cells: HEK293	Sigma	Cat#85120602
Human cells: HEK293S (GnTI−/−)	ATCC	CRL3022
Human cells: HEK293-6E		

(*Continued on next page*)

Continued

REAGENT or RESOURCE	SOURCE	IDENTIFIER
Oligonucleotides		
Recombinant DNA		
CAS9PBKS	Lonowski et al., 2017	Addgene Plasmid#68371
Secrete FcγRIIa reporter construct	This paper	N/A
Secrete MUC1 reporter construct	This paper	N/A
Software and Algorithms		
SysBioWare software	Vakhrushev et al., 2009	N/A
Proteome discoverer 2.2	Thermo Scientific	OPTON-30795

CONTACT FOR REAGENT AND RESOURCE SHARING

Further information and requests from resources and reagents should be directed to and will be fulfilled by the lead Contact, Henrik Clausen (hclau@sund.ku.dk).

METHOD DETAILS

Cell Culture

HEK293 cells (female, SIGMA) were maintained in DMEM (SIGMA) media supplemented with 10% fetal bovine serum (SIGMA) and 4 mM GlutaMAX (GIBCO) at 37°C and 5% CO_2. HEK293-6E were grown in suspension in serum-free F17 culture media (Invitrogen) supplemented with 0.1% Kolliphor P188 (SIGMA) and 4 mM GlutaMax. Cultures were grown at 37°C and 5% CO_2 under constant agitation (120 rpm).

Gene constructs and other reagents

Genes encoding both avian and human hemagglutinin (HA) were amplified from synthesized DNA templates, and HA ectodomains cloned into a customized DNA vector for expression in mammalian tissue culture. Final HA expression constructs with N-terminal CD5 signal peptide for secretion, a C-terminal leucine zipper (GCN4) motif to promote native trimer formation, and HIS8-tag for immobilized metal-affinity chromatography (IMAC) purification. Constructs were transfected into HEK293S (GnTI$^{-/-}$) cells and recombinant HA trimers were purified directly from the culture medium (72 hr) by IMAC. Purified HAs were concentrated and buffer-exchanged to approximately 0.2 - 0.5 mg ml^{-1} in PBS prior to cell-binding assays. GST-tagged ligand-binding regions (GST-BRs) were overexpressed in *E. coli* and purified using Glutathione-Sepharose as described (Bensing et al., 2016).

Transcriptome analysis in HEK293 cell line

RNaseq of HEK293^{WT} cells was performed by deep RNA sequencing using total RNA isolated by standard methods followed by sequencing on an Illumina Hiseq platform using standard protocols (BGI Co, Copenhagen). The RNaseq data resulted in total 4.39 Gb clean bases, which corresponded to 43.9 Mb clean reads. The clean reads were mapped with a total ration of 93.8% to the human reference sequence employing Bowtie2 and RSEM calculation of gene expression levels. A total of 17,364 known genes were detected.

CRISPR/Cas9 targeted KO in HEK293 cells

Knock-out (KO) was performed using a validated gRNA library for all human glycosyltransferases (GlycoCRISPR) (Narimatsu et al., 2018), as previously described (Lonowski et al., 2017). Briefly, HEK293 cells were seeded in 6 well plates (NUNC, Denmark), after one day 1 μg of gRNA was co-transfected with 1 μg of GFP-tagged Cas9-PBKS using Lipofectamine 3000. Cells were harvested after 24 h, and bulk sorted for GFP expression by FACS (SONY SH800). After culturing for 1 week, the sorted cell pool was further single-sorted into 96 well plates and screened by Indel Detection by Amplicon Analysis (IDAA) (Yang et al., 2015a), and select clones were further verified by Sanger sequencing.

ZFN-mediated KI in HEK293 cells

For site-directed knock-in (KI) a modified ObLiGaRe targeted KI strategy utilizing two inverted ZFN binding sites flanking the full coding human glycosyltransferase genes in donor plasmids was used, as described previously (Pinto et al., 2017). KI was performed as described for targeted KO with 1 μg of each ZFN tagged with GFP/Crimson and 3 μg donor plasmid. KI clones were screened by PCR with primers specific for the junction area between the donor plasmid and the AAVS1 locus, and a primer set flanking the targeted KI locus was used to characterize the allelic insertion status.

Stable expression of the GP1bα reporter in HEK293

HEK293^{WT} cells were transfected with an expression construct containing the O-glycosylated stem region of human GP1bα using the same protocol as for KO, and stable clones were selected after G418 selection. A pool was single cell sorted into 96 well plates, and high expressing clones selected by FACS (ECFP) and ICC with an anti-FLAG antibody. Stable clones were used further for KO engineering as listed in Table S1.

Human mucin reporter constructs

A cell membrane reporter construct (MUC-surf-reporter) designed with exchangeable inserts of 150-200 amino acids derived from tandem repeats (TRs) of human mucins was generated by fusion of human MUC1 signal peptide (aa1-62, Uniprot P15921) with 6xHis, Flag-tag, EGFP, multiple cloning site, and the membrane anchoring domain of human MUC1 (aa1042-1138) (Table S2). The multiple cloning site contained EcoRV/PmeI/BamHI/BamHI/NotI/PmeI restriction sites and mucin inserts were synthesized as TrueValue constructs with in-frame BamHI and NotI sites (Genewiz, USA). The MUC1 secreted reporter construct was synthesized with NotI/XhoI and a 10xHis STOP encoding ds oligo (5′-GCGGCCGCCCATCACCACCATCATCACTGATAGCGCTCGAG-3′, NotI/XhoI restriction sites underlined). All constructs were Sanger sequence verified. Transient expression in HEK293 cells was performed one day after seeding cells into 24 wells, and transfected cells were harvested 48 h post-transfection and used for binding studies.

Cell binding assays

Cell binding assays were performed on ice with mAbs, lectins, precomplexed glycan-binding proteins, Siglecs and influenza virus HAs. Biotinylated lectins (Vector Laboratories, Burlingame, CA) were incubated at different concentrations for 1 h, followed by washing and incubation with Streptavidin-Alexa Fluor488 (Invitrogen) for 1 h. Recombinant human Siglec Fc-chimera (R&D systems, Minneapolis, MN) were precomplexed with Alexa Fluor647 goat anti-human IgG antibody (Life Technologies) for 1 h followed by incubation with cells for 1 hr. His-tagged HAs were precomplexed for 45 min with anti-6xHis mouse IgG (Thermo) and Alexa Fluor647 goat anti-mouse IgG (Invitrogen) in 4:2:1 ratio followed by incubation with cells for 3 h. HEK293 cells stably expressing GP1bα or transiently expressing mucin reporter constructs were incubated with GST-BRs at different concentrations for 1 h, followed by washing, and incubation with rabbit polyclonal anti-GST (Thermo) for 1 h, and further incubated with Alexa Fluor647 goat anti-rabbit IgG antibody (Life Technologies) for 1 h. Washing was performed with 1% BSA/PBS and cells were resuspended for flow cytometry analysis (SONY SA3800). Testing of different concentrations of precomplexed reagents was performed by diluting the complexes in 1% BSA/PBS.

Production of N- and O-glycosylation reporter proteins

A reporter for N-glycosylation was designed as a secreted construct of the FcγRIIa N-glycoprotein, encoding the extracellular domain (aa1-217, Uniprot P12318) fused with a 10xHis tag. Secreted FcγRIIa was transiently produced in suspension HEK293-6E cells. Briefly, 30 mL of HEK293-6E cells were seeded at a cell density of 0.5 × 10^6 cells/ml and transfected the next day with 30 μg of the secrete FcγRIIa construct and 90 μg of PEI (1:3 ratio) incubated at room temp. for 15 min and cultured for 72 h before harvest. A reporter for GalNAc-type O-glycosylation was designed as a secreted construct of the mucin MUC1 encoding TRs (also used for the mucin display). The reporter was stable expressed in HEK293-6E after G418 selection, and a stable pool of cells were seed at a cell density of 1.0 × 10^6 cells/ml and cultured 72 h. Secreted FcγRIIa and MUC1 were purified from culture medium by nickel affinity chromatography. Media was mixed 3:1 (v/v) in 4 × binding buffer (100 mM sodium phosphate, pH 7.4, 2 M NaCl) and applied to self-packed nickel-nitrilotriacetic acid (Ni-NTA) affinity resin column (QIAGEN), pre-equilibrated in washing buffer (25 mM sodium phosphate, pH 7.4, 500 mM NaCl, 20 mM imidazole). After washing, bound protein was eluted with 200 mM imidazole in washing buffer. The protein containing fractions were identified by SDS-PAGE, and further purified by reverse-phase HPLC with a Jupiter 5 μ C4 300A column (Phenomenex, Torrence, CA), using 0.1% trifluoroacetic acid (TFA) and a gradient of 10%–100% acetonitrile.

Sample preparation for site-specific N-glycopeptide analysis

20 μg of the purified FcγRIIa was dissolved in 50 mM ammonium bicarbonate (AmBic) buffer, reduced in 10 mM dithiothreitol (DTT) at 60°C for 45 min, alkylated (20 mM iodoacetamide (IAA), in the dark at RT for 30 min), reduced again (10 mM DTT, 20°C, RT) and digested with 0,8 U chymotrypsin (1:25 ratio chymotrypsin:protein) (Roche) (25°C, 4 h). The proteolytic digest was desalted by in-house produced modified StageTip columns containing 3 layers of C18 membrane (3M Empore disks from Sigma Aldrich) (Rappsilber et al., 2007). Samples were eluted with 50% methanol in 0.1% formic acid (FA), dried in SpeedVac and re-solubilized in 0.1% FA and submitted for LC MS/MS analysis.

Sample preparation for total cell lysate N-glycan analysis

The packed cell pellets (1x10^7 cells) were lysed in 1 mg Rapigest SF Surfactant (Waters), in 50 mM AmBic and homogenized by sonication. Cleared lysates were heated (95°C, 15 min), diluted in 50 mM AmBic to a final concentration of 0.2% Rapigest and sonicated again followed by reduction (10 mM DTT, 60°C, 45 min), alkylation (20 mM iodoacetamide, in the dark at RT for 30 min), reduction

(10 mM DTT, RT, 20 min) and digested with 25U trypsin (Roche) in 50mM AmBic (37°C, 12 h, 650 rpm). Each tryptic digest was acidified with TFA and incubated at 37°C for 30 min before centrifuging (max speed, RT, 15 min). Sep-Pak C18 columns (Waters) where washed with 100% methanol, 50% methanol 0.1% FA and equilibrated with 0.1% trifluoroacetic acid (TFA) before loading the supernatants containing the tryptic digests. After reloading the flow through, the column was washed with 0.1% TFA, twice with 0.1% FA and eluted twice with 50% methanol 0.1% FA. 10 ug of Freeze-dried samples were resuspended in 50 mM AmBic with 8U PNGaseF (Roche) and incubated at 37°C for 16 h. The digest was applied to Sep-pak C18 column, as described above, and flow through containing the released N-glycans was collected for further labeling with Rapifluor-MS glycan kit (Waters) as described by manufacturers.

Sample preparation for O-glycopeptide analysis

Approximately 50 μg of the purified MUC1 reporter was reduced, alkylated and digested with 10 μg endo-AspN (Roche) (37°C, O/N). The digested sample was fractionated by C18 HPLC, and the MUC1 20-mer TR glycopeptide identified and analyzed by LC-MS/MS.

Mass Spectrometry

LC MS/MS analysis was performed on EASY-nLC 1200 UHPLC (Thermo Scientific) interfaced via nanoSpray Flex ion source to an Orbitrap Fusion Lumos MS (Thermo Scientific). Briefly, the nLC was operated in a single analytical column set up using PicoFrit Emitters (New Objectives, 75 μm inner diameter) packed in-house with Reprosil-Pure-AQ C18 phase (Dr. Maisch, 1.9-μm particle size, 19-21 cm column length). Each sample was injected onto the column and eluted in gradients from 3 to 32% B for glycopeptides, and 10 to 40% for released and labeled glycans in 45 min at 200 nL/min (Solvent A, 100% H_2O; Solvent B, 80% acetonitrile; both containing 0.1% (v/v) formic acid). A precursor MS1 scan (m/z 350–2,000) of intact peptides was acquired in the Orbitrap at the nominal resolution setting of 120,000, followed by Orbitrap HCD-MS2 and at the nominal resolution setting of 60,000 of the five most abundant multiply charged precursors in the MS1 spectrum; a minimum MS1 signal threshold of 50,000 was used for triggering data-dependent fragmentation events. Targeted MS/MS analysis was performed by setting up a targeted MS^n (tMS^n) Scan Properties pane. A target list was composed from top 30 most abundant glycans or glycopeptides from the proposed compositional list (Table S3).

Data Analysis

Glycan and glycopeptide compositional analysis was performed from *m/z* features extracted from LC-MS data using in-house written SysBioWare software (Vakhrushev et al., 2009). For *m/z* feature recognition from full MS scans LFQ Profiler Node of the Proteome discoverer 2.2 (Thermo Scientific) was used. The list of precursor ions (m/z, charge, peak area) was imported as ASCII data into SysBioWare and compositional assignment within 3 ppm mass tolerance was performed. The main building blocks used for the compositional analysis were: NeuAc, Hex, HexNAc, dHex and the theoretical mass increment of the most prominent peptide corresponding to each potential glycosites. The most prominent peptide sequences related to N-glycosites of interest were determined experimentally by comparing the yield of deamidated peptides with and without PNGase F treatment. One or two phosphate groups were added as building blocks for assignment. To generation the potential glycopeptide list, all the glycoforms with an abundance higher than 10% of the most abundant glycoform were used for glycan feature analysis. All high mannose and hybrid structures were excluded in the TCL data.

Disaccharide analysis of GAGs

Disaccharide composition analysis was performed with a panel of bacterial polysaccharide lyases (R&D Systems) and 2-aminoacridone (AMAC) labeling on a Waters Acquity UPLC system equipped with a fluorescence (FLR) detector as described previously (Ref Nature method). The 500 μl packed cell pellets from 5 million cells were resuspended in a lysis buffer containing 50 mM Tris-HCl buffer, pH 7.6, 10 mM $CaCl_2$, 0.1% Triton X-100, and 1 mg/ml Pronase (Roche) in a total volume of 1 ml. Reactions were incubated at 37°C overnight with end-to-end rotation, and heated at 100°C for 10 min to inactivate Pronase; after centrifugation, supernatants were adjusted to 2 mM $MgCl_2$, mixed with 250 U of Benzonase (Sigma), and incubated at 37°C for 2 h. Reactions were acidified with acetic acid to pH 5.0 and loaded onto a Q-Sepharose column (0.5 ml) (Sigma) equilibrated with 20 mM sodium acetate, pH 5.0, 100 mM NaCl, and 0.1% Triton X-100. The column was washed first with the equilibration buffer and then with the same buffer without Triton X-100 to remove the detergent. The bound GAG fraction was eluted with 1.5 mL of buffer containing 20 mM sodium acetate, pH 5.0, and 1 M NaCl and pelleted by ethanol precipitation and dissolved in de-ionized water. For evaluation of total CS/DS, chondroitinase ABC (10 mU) was used for digestion in 40 mM sodium acetate and 1 μM $CaCl_2$ at 37°C overnight. For the evaluation of HS, a mixture of heparinases I, II, and III, or of II and III only (10 mU of each), was used in 40 mM sodium acetate and 5 mM CaCl2 at 37°C overnight. Released disaccharides were dissolved in 5 μL of 0.1 M AMAC solution in glacial acetic acid–DMSO (vol/vol 3:17) and incubated at room temperature for 15 min, followed by mixing with 5 μL of 1 M $NaCNBH_3$ and further incubation at 45°C for 3 h. Excess AMAC was removed by acetone precipitation. Labeled disaccharides corresponding to 0.5 million cells were subsequently analyzed on a Waters Acquity UPLC system equipped with a fluorescence (FLR) detector. The separation was optimized on a BEH C18 column (2.1 Å ~150 mm, 1.7 μm; Waters) at 30°C for CS/DS and 40°C for HS, with 80 mM ammonium acetate as mobile phase A (pH 5.5) for CS/DS and 150 mM ammonium acetate as mobile phase A (pH 5.6) for HS, and with 100% acetonitrile as mobile phase B

for CS/DS and HS. Separation of the disaccharides was performed with a gradient of mobile phase B increasing from 3 to 13% over 30 min at a flow rate of 0.2 ml/min. Each series of HPLC runs was preceded with standards (20 pmol AMAC-labeled disaccharides; Iduron).

DATA AND SOFTWARE AVAILABILITY

The mass spectrometry proteomics data have been deposited to the ProteomeXchange Consortium via the PRIDE repository with the dataset identifier PXD013676.